DIGITAL IMAGE PROCESSING OF REMOTELY SENSED OCEANOGRAPHIC DATA

MÜŞERREF TÜRKMEN

AUGUST 2008

DIGITAL IMAGE PROCESSING OF REMOTELY SENSED
OCEANOGRAPHIC DATA

A THESIS SUBMITTED TO
THE GRADUATE SCHOOL OF APPLIED MATHEMATICS
OF
THE MIDDLE EAST TECHNICAL UNIVERSITY

BY

MÜŞERREF TÜRKMEN

IN PARTIAL FULFILLMENT OF THE REQUIREMENTS FOR THE
DEGREE OF
MASTER OF SCIENCE
IN
THE DEPARTMENT OF SCIENTIFIC COMPUTING

AUGUST 2008

Approval of the Graduate School of Applied Mathematics

———————————————

Prof. Dr. Ersan AKYILDIZ
Director

I certify that this thesis satisfies all the requirements as a thesis for the degree of
Master of Science.

———————————————

Prof. Dr. Bülent KARASÖZEN
Head of Department

This is to certify that we have read this thesis and that in our opinion it is fully
adequate, in scope and quality, as a thesis for the degree of Master of Science.

———————————————   ———————————————
Assist. Prof. Dr. Hakan ÖKTEM   Prof. Dr. Bülent KARASÖZEN
Supervisor   Co-supervisor

Examining Committee Members

Assoc. Prof. Dr. Azize HAYFAVİ   ———————————————

Assist. Prof. Dr. Hakan ÖKTEM   ———————————————

Prof. Dr. Gerhard Wilhelm WEBER   ———————————————

Assoc. Prof. Dr. Emrah ÇAKÇAK   ———————————————

Assist. Prof. Dr Fahd JARAD   ———————————————

I hereby declare that all information in this document has been obtained and presented in accordance with academic rules and ethical conduct. I also declare that, as required by these rules and conduct, I have fully cited and referenced all material and results that are not original to this work.

Name, Last name: Müşerref TÜRKMEN

Signature:

ABSTRACT

DIGITAL IMAGE PROCESSING OF REMOTELY SENSED OCEANOGRAPHIC DATA

TÜRKMEN, Müşerref

M.Sc., Department of Scientific Computing

Supervisor: Assist. Prof. Dr. Hakan ÖKTEM

Co-supervisor: Prof. Dr. Bülent KARASÖZEN

August 2008, 106 pages

Developing remote sensing instrumentation allows obtaining information about an area rapidly and with low costs. This fact offers a challenge to remote sensing algorithms aimed at extracting information about an area from the available remote sensing data. A very typical and important problem being interpretation of satellite images. A very efficient approach to remote sensing is employing discriminant functions to distinguish different landscape classes from satellite images. Various methods on this direction are already studied. However, the efficiency of the studied methods are still not very high. In this thesis, we will improve efficiency of remote sensing algorithms. Besides we will investigate improving boundary detection methods on satellite images.

Keywords: remote sensing, sea surface temperature, image processing, mathematical morphology, edge detection, segmentation, reconstruction.

ÖZ

UZAKTAN ALGILANAN OKYANUS VERİLERİNDE SAYISAL GÖRÜNTÜ İŞLEME

TÜRKMEN, Müşerref

Yüksek Lisans, Bilimsel Hesaplama Bölümü

Tez Danışmanı: Assist. Prof. Dr. Hakan ÖKTEM

Tez Yardımcısı: Prof. Dr. Bülent KARASÖZEN

Ağustos 2008, 106 sayfa

Uzaktan Algılama araçları geliştirmek daha az maliyetle daha hızlı bilgi edinmemize olanak tanır. Bu nedenle geliştirilmiş uzaktan algılama algoritmaları kullanılabilir uzaktan algılama verileri sayesinde bilgi edinmeyi daha kolaylaştırmayı amaçlar. Uydu görüntülerini yorumlamak önemli bir problemdir. Uzaktan algı lamada diskriminant fonksiyonlarını kullanarak uydu görüntülerinden değişik alanları ayırt etmek çok etkili bir yöntemdir. Bu yöndeki çeşitli metotlar araştırılmıştır. Ancak çalışılan yöntemlerin performansı hala çok yüksek değildir. Bu tezde, uzaktan algılama metotlarının performansını artıracağız. Ayrıca sınırlı algılama algoritmalarının geliştirilmesini araştıracağız.

Anahtar Kelimeler: uzaktan algılama, deniz yüzeyi sıcaklığı, görüntü işleme, matematiksel morfoloji, sınır bulma, kesimleme, yeniden yapılandırma.

To my parents

ACKNOWLEDGEMENTS

I do not have enough words to express how thankful I am to my advisor Assist. Prof. Dr. Hakan Öktem for his supervision, advice, patiently guiding, motivating and especially the encouragement he has given me throughout this study.

I am thankful to my co-supervisor Prof. Dr. Bülent Karasözen for his kindness and suggestions throughout this study.

I am grateful to my inspiration Mustafa Düzer for gathering all the data used in this thesis, always being by my side and supporting me during this long process.

I want to thank my dear friend Hatice who offered her help and support continuously me since the first day of this project.

I also want to thank my dear friends Mustafa, Önder, Derya, Nurgül and Nilüfer for their endless support and being with me all the time.

I thank the members of IAM for all their constructive comments and their support.

I am grateful the member of IMS especially Murat, Serkan and Hasan for introducing me to atmospheric science and oceanography and making research in this field seem so exciting. They offered me so generously a perfect working environment, support, and help whenever I needed it. I feel so lucky for just having the opportunity to work with them and learn from them, during my studies.

Finally I would like to thank my dear family for always being by my side, for their understanding and patient dispositions, and their endless support. Without them this thesis would have never been written.

TABLE OF CONTENTS

LIST OF FIGURES

LIST OF TABLES

CHAPTER 1

INTRODUCTION

1.1   Objectives

Remote sensing and other satellite measurements in recent years have provided meteorologists, oceanographers and geodesists with new techniques for observations. The accuracy of satellite observations of the ocean surface is the reason we choice satellite derived data, i.e., Spatial resolution = 1km.

One of the most important contributions of satellite remote sensing to climate studies is the establishment of global *sea surface temperature (SST)* data sets. One use of regular global SST data is to test estimates of global warming due to increases in atmospheric carbon dioxide. Another use of SST data sets is to detect SST anomalies, which are associated with changes in atmospheric circulation and hence the weather. In addition to them SST data have many use in oceanography and more proper data give more suitable result. Namely, if we are able to improve the efficiency of processing techniques we can provide more accurate data so one can get better result of usage of SST.

In this thesis we aimed at: realizing the reasons of imperfectness of processing algorithms for oceanographic data and reducing these reasons to get better results.

1.2 Thesis Outline

Unless we know what remote sensing is, we can not apply nor understand digital image processing (DIP) properly. To make this study more comprehensible, in Chapter 2, we give some basic definitions and properties of remote sensing and remote sensor systems. Also a review of the history and methods associated with the satellite observations of the ocean is presented in this chapter.

Chapter 3, introduces the mathematical background of the study such as linear algebra, numerical analysis and mathematical morphology. We use and develop various methods based on these subjects to improve or apply digital image processing algorithms. We study interpolation and curve fitting techniques useful not only for image enhancement but also in the reconstruction methods. Mathematical morphology is a very important task for all DIP techniques, we discuss morphological techniques in Chapter 3 and Chapter 5.

Chapter 4, gives information about digital image processing and examines DIP techniques with presenting three important processing procedures used in this study. In Section 1, edge detection techniques are presented and compared with respect to efficiency but none of them find all edges in a sea surface temperature (SST) data because of incompleteness and roughness of data. Since this imperfection is caused by our data, we tried to fix our data using reconstruction. Note that before reconstruction, we used histogram mapping method to improve the reconstruction method's result.

In Section 2, some of the well-known segmentation techniques presented and advantages/disadvantages of these techniques are mentioned. A new image segmentation technique based on edge tracing algorithm is used to segmentation of data. This technique give more convenient segments in contrary to other methods included in this chapter.

Reconstruction is the most problematic phase of digital image processing of ocean data. In Section 3, we briefly summarized that why reconstruction is so difficult when data are remotely sensed from ocean.

In Chapter 5 we explain why we need new techniques and introduces our techniques' basis while compare the methods with some convenient methods. This chapter represents an adaptive histogram modification algorithm, a segmentation algorithm and a reconstruction algorithm with figures.

THEORETICAL BACKGROUND

2.1 Introduction to Remote Sensing

Remote sensing is the science of gathering information from a distance, and it provides a descriptive, analytical way to identify geographic features. Remote sensing uses such technology as aerial photography and satellite imagery to record information about features on the land and in the water [46]. The remotely collected data can be of many forms, including variations in force distributions, acoustic wave distributions, or electromagnetic (EM) energy distributions [46, 47]. In much of remote sensing, the process involves an interaction between incident radiation and the targets of interest. This is exemplified by the use of imaging systems where the following seven elements are involved.

A. *Energy Source or Illumination* - the first requirement for remote sensing is to have an energy source which illuminates or provides electromagnetic energy to the target of interest.

B. *Radiation and the Atmosphere* - as the energy travels from its source to the target, it will come in contact with and interact with the atmosphere it passes through. This interaction may take place a second time as the energy travels from the target to the sensor.

C. *Interaction with the Target* - once the energy makes its way to the target through the atmosphere, it interacts with the target depending on the properties

of both the target and the radiation.

D. *Recording of Energy by the Sensor* - after the energy has been scattered by, or emitted from the target, we require a sensor (remote - not in contact with the target) to collect and record the electromagnetic radiation.

E. *Transmission, Reception, and Processing* - the energy recorded by the sensor has to be transmitted, often in electronic form, to a receiving and processing station where the data are processed into an image.

F. *Interpretation and Analysis* - the processed image is interpreted, visually and/or digitally or electronically.

G. *Application* - the final element of the remote sensing process is achieved when we apply the information we have been able to extract from the imagery about the target in order to better understand it, reveal some new information, or assist in solving a particular problem [46].
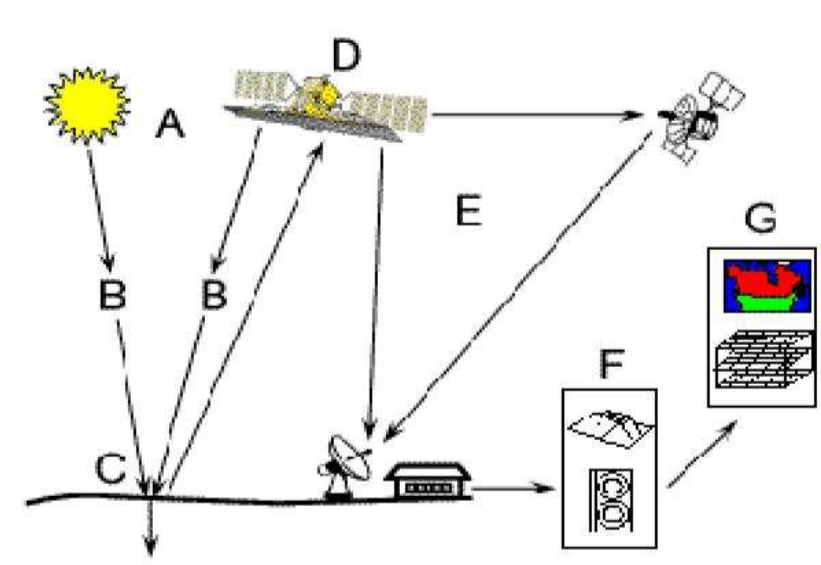
Figure 2.1: Remote sensing system.

Remotely sensed data are regularly used in many areas such as weather forecasting, archaeology, biology, oceanography, coastal observation, etc. While remote sensing is a valuable research tool, it has limitations. Resolution is limited by how much information can be gathered and processed. A remote sensor may assign a single value to a pixel, while in reality there is a lot of variety inside that area. Students and scientists who use remote sensing have to deal with a two-fold problem: how to get more information than the image may show; and how to verify that the information from the remote sensor is accurate. Furthermore, a digital device is only taking samples of an analog signal, it is not actually copying the entire signal. Some of the original signal is always left out. Thus scientists have developed ways to use computers to reconstruct the missing data between samples.

Two characteristics of electromagnetic radiation - energy required for RS - inversely related to each other are important for understanding remote sensing. These are the wavelength and frequency. The wavelength is the length of one wave cycle, which can be measured as the distance between successive wave crests. Frequency refers to the number of cycles of a wave passing a fixed point per unit of time. Frequency is normally measured in hertz (Hz), equivalent to one cycle per second, and various multiples of hertz [47].

The electromagnetic spectrum categorizes electromagnetic waves by their wavelengths. The most important wavelengths for remote sensing are:

the visible wavelengths:

- blue: 0.4 - 0.5 μm

- green: 0.5 - 0.6 μm

- red: 0.6 - 0.7 μm

near infrared: 0.7 - 1.1 μm;

short-wave infrared: 1.1 - 2.5 μm;

thermal infrared: 3.0 14.0 μm;

microwave region: 103 - 106 μm or 1 mm to 1 m.

Before light and radiation reach a remote sensing system, atmosphere can have a profound effects caused by the atmospheric scattering and absorption. Scattering occurs when particles or large gas molecules present in the atmosphere interact with and cause the electromagnetic radiation to be redirected from its original path, i.e. degradation of image quality for earth observation. Absorption is the other main mechanism at work when electromagnetic radiation interacts with the atmosphere. In contrast to scattering, this phenomenon causes molecules in the atmosphere to absorb energy at various wavelengths [46].

In remote sensing, we are most interested in measuring the radiation reflected from targets. When the EM energy reaches the Earth surface, the total energy will be broken into three parts: reflected, absorbed, and/or transmitted. Some energy is absorbed by vegetation, bare ground, water, etc. How much energy is absorbed depends on the wavelength, or frequency. If an object reflected all energy, it would look like a mirror. If it absorbed all energy, it would look completely black. Many objects transmit at least some of the energy they receive. The combination of absorption, reflection, and transmission of various light frequencies are what makes objects appear to us.

We often use humanmade energy source to illuminate the target (such as radar) and to collect the backscatter from the target. A remote sensing system relying on human-made energy source is called an "active" remote sensing system. Remote sensing relying on energy sources which is not human-made is called "passive" remote sensing. Advantages for active sensors include the ability to obtain measurements anytime, regardless of the time of day or season. Working mechanism of sensors can be summarized as follows. The information from a narrow wavelength range is gathered and stored in a channel, also sometimes referred to as a band. We can combine and display channels of information digitally using the three primary colours (blue, green, and red). The data from each channel is represented as one of the primary colours and, depending on the relative brightness

(i.e., the digital value) of each pixel in each channel, the primary colours combine in different proportions to represent different colours.

An image refers to any pictorial representation, regardless of what wavelengths or remote sensing device has been used to detect and record the electromagnetic energy [46]. Each picture element in an image, called a pixel, has coordinates of (x, y) in the discrete space representing a continuous sampling of the earth surface. Image pixel values represent the sampling of the surface radiance. Pixel value is also called image intensity, image brightness or grey level. In a multispectral image, a pixel has more than one grey level. Each grey level corresponds to a spectral band. These grey levels can be treated as grey-level vectors.

Successful image applications of remotely sensed data requires careful attention to both the remote sensor systems and environmental characteristics. Among various factors that affect the quality and information content of remotely sensed data, two concepts are extremely important for us to understand. They determine the level of details of the modeling process. These are the resolution and the sampling frequency.

Resolution is a measure of the ability of an optical system to distinguish between signals that are spatially near or spectrally similar. *Spectral resolution* refers to the number and dimension of specific wavelength intervals in the electromagnetic spectrum to which a sensor is sensitive. Careful selection of the spectral bands may improve the probability that a feature will be detected and identified and biophysical information extracted. *Spatial resolution* is a measure of the smallest angular or linear separation between two objects that can be resolved by sensor. There is a relationship between the size of a feature to be identified and the spatial resolution of the remote sensing system. Generally the smaller the spatial resolution is the greater the resolving power of the sensor system. The *temporal resolution* of a sensor system refers to how often it records imagery of a particular area. *Radiometric resolution* defines the sensitivity of a detector to differences in signal strength as it records the radiant flux reflected or emitted from the region of interest. Improvement in resolution generally increase the probability that

phenomena can be remotely sensed more accurately [50].

For high spatial resolution, the sensor has to have a small IFOV. However, this reduces the amount of energy that can be detected as the area of the ground resolution cell within the IFOV becomes smaller. This leads to reduced radiometric resolution - the ability to detect fine energy differences. To increase the amount of energy detected (and thus, the radiometric resolution) without reducing spatial resolution, we would have to broaden the wavelength range detected for a particular channel or band. Unfortunately, this would reduce the spectral resolution of the sensor. Conversely, coarser spatial resolution would allow improved radiometric and/or spectral resolution. Thus, these three types of resolution must be balanced against the desired capabilities and objectives of the sensor [46].

2.2   Introduction to Satellites

In order for a sensor to collect and record energy reflected or emitted from a target or surface, it must reside on a stable platform removed from the target or surface being observed. Platforms for remote sensors may be situated on the ground, on an aircraft or balloon (or some other platform within the Earth's atmosphere), or on a spacecraft or satellite outside of the Earth's atmosphere. The big advantage of satellite remote sensing is that it provides for coverage in space and time on a scale that is not otherwise achievable [46].

Satellites at very high altitudes, which view the same portion of the Earth's surface at all times have geostationary orbits. From a satellite in geostationary orbit at 35000 km altitude directly above a fixed point on the equator, continuous observation of about a quarter of the atmosphere is possible. This allows the satellites to observe and collect information continuously over specific areas. Weather and communications satellites commonly have these types of orbits. Interpretation of these remote sounding observations is often complex and difficult, but they posses the enormous advantage, compared with conventional and in situ observations, that a satellite can provide observations over a very large area in a

short time [50].

As a satellite revolves around the Earth, the sensor "sees" a certain portion of the Earth's surface. The area imaged on the surface, is referred to as the swath (Figure 2.3).
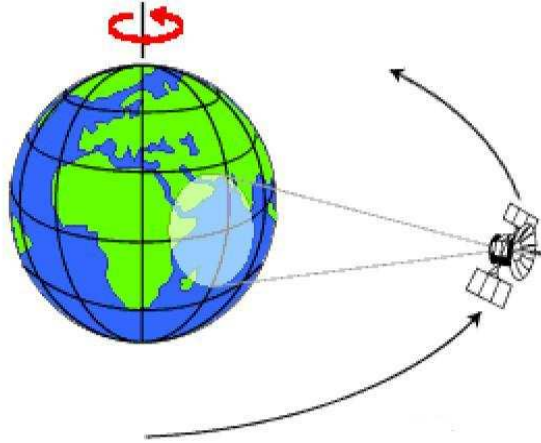
Figure 2.2: Satellite orbit and swath.

Many remote sensing platforms are designed to follow an orbit (basically north-south) which, in conjunction with the Earth's rotation (west-east), thus the satellite is shifting westward. This apparent movement allows the satellite swath to cover a new area with each consecutive pass [50].

Definition The *Instantaneous Field of View (IFOV)* is the angular cone of visibility of the sensor and determines the area on the Earth's surface which is "seen" from a given altitude at one particular moment in time. The size of the area viewed is determined by multiplying the IFOV by the distance from the ground to the sensor. [46]

Common satellites and their some properties are listed below. For more information see [47].

2.2.1 NOAA-AVHRR

The first satellite for remote sensing observations was launched in 1960 and was called *TIROS (Television and Infrared Observation Satellite)*. It was developed for meteorological purposes by the *National Oceanic and Atmospheric Administration (NOAA)* of the USA. *AVHRR* stands for *Advanced Very High Resolution Radiometer* and was also built for meteorological observation. It has a near-polar, sun-synchronous orbit at an altitude of approximately 830 k. It has the following five spectral bands:

1) 0.58 - 0.68 μm

2) 0.72 - 1.10 μm

3) 3.55 - 3.93 μm

4) 10.5 - 11.5 μm

5) 11.5 - 12.5 μm

Altitude: 830 k

Orbit incl.: 98.9°

Repeat time: 1 day

IFOV: $\pm$ 1.1 k

2.2.2 NIMBUS

The first *NIMBUS* was launched in 1964 and NIMBUS-7 was put in orbit in 1978, was developed by NASA for meteorological and oceanographic research: measuring sea water temperature, to map phytoplankton concentration and suspended materials. NIMBUS has the following six spectral bands:

1) 0.43 - 0.45 μm

2) 0.51 - 0.53 μm

3) 0.54 - 0.56 μm

4) 0.66 - 0.68 μm

5) 0.70 - 0.80 μm

6) 10.5 - 12.5 μm

Altitude: 910 k

Orbit incl.: $\pm 98°$

IFOV: $\pm$ 800 m

2.2.3   Metosat

This satellite is operated by the *European Space Agency (ESA)* and is located on a fixed position above the Greenwich Meridian over West Africa. Meteosat-1 was launched in November 1977. The Meteosat record images every 30 minutes in three wavelengths in visible and near-infrared, in the water vapour absorption region and in the thermal infrared. Due to their poor spatial resolution, environmentalists rarely use the meteosat images.

1) 0.4 - 1.1 μm

2) 5.7 - 7.1 μm

3) 10.5 - 12.5 μm

Altitude: 35.786 k

Record image every 30 minutes

Pixelsize: 2.5 - 5.0 k

2.2.4   LANDSAT

The American *Landsat* series of satellites (*Landsat MSS, Landsat TM and Landsat ETM+*) were developed within the Earth Resources Programme of NASA in the early seventies. The first *Landsat* satellite was launched on 22 July 1972. This satellite was of great importance because it provided many, high quality beautiful images which gave remote sensing technology world-wide recognition. The Landsat satellites all carry or have carried aboard a multi-spectral scanning system MSS. The Landsat satellites are in an orbit at an altitude of approximately 900 km (later lowered to 700 km) and the MSS and TM sensors provide images of 185 by 185 km. MSS provides images in 64 grey levels (6 bits), TM sends down images in 256 grey levels (8 bits). The Landsat satellites have a sun-synchronous orbit with an inclination of 98.2, they require approximately 100 minutes to circle the earth and they have a repeat time of 16 days.

1) 0.45-0.52 Blue: Designed for water body penetration

2) 0.52-0.60 Green: designed to measure green reflectance peak of vegetation

3) 0.63-0.69 Red: designed to sense in chlorophyll absorption bands for species differentiation.

4) 0.76-0.90 Near infrared: useful for determining vegetation types, vigour and biomass content and for delineating water bodies.

5) 1.55-1.75 Short-wave infrared: Indicative of vegetation moisture content and soil moisture. Useful to discriminate clouds from snow.

6) 10.4-12.5 Thermal infrared: Useful in vegetation stress analysis, soil moisture mapping and thermal mapping.

7) 2.08-2.35 Short-wave infrared: Useful for discrimination of mineral and rock types.

2.2.5 IKONOS

IKONOS is developed, built and maintained by the company *Space Imaging*. The sensor aboard Ikonos has a panchromatic band with a spatial resolution of 1 by 1 meter. Next it has a sensor with four multi-spectral bands: blue, green, red, and infrared of 4 by 4 meters.

IKONOS- Panchromatic:

1) 450 900 nm

IKONOS XS:

1) 450 520 nm (Blue)

2) 520 600 nm (Green)

3) 630 690 nm (Red)

4) 760 900 nm (NIR)

Orbit altitude: 681 km Orbit swath: 11 km

2.2.6 CZCS

The *Coastal Zone Color Scanner (CZCS)* was designed specifically to measure the color and temperature of coastal zones of the oceans. The system had a 1566 km swath width and an 825 m resolution at nadir. The first four visible bands of the CZCS were very narrow and centered to enhance the discrimination of very subtle water reflectance differences. The CZCS was used to successfully detect chlorophyll, temperature, suspended solids and yellow substance in the combinations and concentrations typical of near-shore and coastal waters. The CZCS ceased operation in 1986.

1) 0.43 - 0.45 μm (Chlorophyll absorption)

2) 0.51 - 0.53 μm (Chlorophyll absorption)

3) 0.54 - 0.56 μm (Yellow substance)

4) 0.66 - 0.68 μm (Chlorophyll concentration)

5) 0.7 - 0.8 μm (Surface vegetation)

6) 10.5 - 12.5 μm (Surface temperature)

2.3 MODIS (Moderate Resolution Imaging Spectroradiometer)

MODIS (Moderate Resolution Imaging Spectroradiometer) is a key instrument aboard the *Terra (EOS AM)* and *Aqua (EOS PM)* satellites. MODIS is designed for monitoring large-scale changes in the biosphere that will yield new insights into the workings of the global carbon cycle. MODIS can measure the photosynthetic activity of land and marine plants (phytoplankton) to yield better estimates of how much of the greenhouse gas is being absorbed and used in plant productivity. Coupled with the sensor's surface temperature measurements, MODIS' measurements of the biosphere are helping scientists track the sources and sinks of carbon dioxide in response to climate changes (MODIS, 2003). MODIS can be thought of as a highly improved successor to NOAA AVHRR and CZCS. MODIS not only provide two-day repeat global coverage but also collect data in 36 carefully chosen spectral bands. MODIS is scheduled to orbit at an altitude of 705 km and have to a total field of view of $\pm 55°$, providing a data swath width of 2330 km.

Given the enormous expanse of Earths oceans, their crucial role in climate change is not surprising. Oceans absorb solar radiation and modulate the Earths temperature, they exchange gases with the atmosphere, and they harbor an astounding diversity of plants and animals, many of which human cultures all over the world depend on for food. One way MODIS helps scientists studying oceans is through collection of data that they can use to make global maps of ocean color.

Temperature

Temperature in the ocean varies widely, both horizontally and with depth. Maximum values of about 32° C are encountered at the surface in the Persian Gulf in summer, and the lowest possible values of about −2° C; the usual minimum freezing point of seawater) occur in polar regions.

In addition to ocean color measurements that tell scientists about ocean productivity and carbon movement, MODIS is taking daily global measurements of *sea surface temperature (SST)*. SST is important to the study of global change for many reasons. The exchange of heat, moisture, and gases between the ocean and the atmosphere determines Earths habitability, and SST largely determines the rate of exchange. The rate at which carbon dioxide dissolves in water is temperature dependent, as is the rate of water evaporation. Since water vapor is a potent greenhouse gas, the rate of evaporation is an important factor in climate change. SST also factors into cloud formation, including thunderstorms and hurricanes (see MODIS homepage for more detail).

2.3.1 Preprocessing of Data

It is often necessary to perform a number of operations on the collected remote sensing data in order to create an image that is a good representation of the reality and that is useful for quantitative or qualitative estimates of variables. This typically involves a correction for geometrical distortions, a radiometric calibration of the data and removal of the influence of the atmosphere. The most common satellite image product includes correction for earth rotation, spacecraft altitude, attitude and sensor variations [46, 47].

Histogram

In an image processing context, the histogram of an image normally refers to a histogram of the pixel intensity values. This histogram is a graph showing the

number of pixels in an image at each different intensity value found in that image. For an 8-bit grayscale image there are 256 different possible intensities, and so the histogram will graphically display 256 numbers showing the distribution of pixels amongst those grayscale values.

When one wishes to compare two or more images on a specific basis, it is common to first normalize their histograms to a "standard" histogram. This can be especially useful when the images have been acquired under different circumstances. The most common histogram normalization technique is histogram equalization where one attempts to change the histogram through the use of a function $b = f(a)$ into a histogram that is constant for all brightness values. This would correspond to a brightness distribution where all values are equally probable. The histogram derived from a local region can also be used to drive local filters that are to be applied to that region. Examples include minimum filtering, median filtering, and maximum filtering.

Geometric correction

Remote sensing images initially contain a number of geometric distortions that are a result of the data recording procedure and the shape and rotation of the earth. Geometric correction is the process of correcting for such distortions and the distortions in the image can be corrected by transformation of the image to the geometry of the chosen map projection, i.e., via ground control points. Expressing this in mathematic notation,

$$x = f_1(X, Y)$$

$$y = f_2(X, Y),$$

where

$(x, y)=$ distorted image coordinates (column, row),

$(X, Y)=$ correct (map) coordinates,

f_1, f_2 =transformation functions.

Note that some of the geometric distortions are usually corrected for by the data distributor before delivery [47].

Radiometric correction

Digital images are a set of two dimensional rasters of *digital numbers* (DN). Conversion of DNs to absolute radiance values - for any given channel - are computed from

$$DN = gL + o, \tag{2.3.1}$$

where

g = channel gain (slope),

L = spectral radiance measured over the spectral bandwith of the channel,

o = channel offset (intercept).

Major sources of error in the radiometric determination are (a) sun glint (MODIS bands 20, 22, and 23), (b) water vapor absorption in the atmosphere (MODIS bands 31, 32), [atbd mod25]. Total spectral radiance [47] can be expressed by

$$L_{tot} = \frac{\rho E T}{\pi} + L_p, \tag{2.3.2}$$

where ρ = reflectance of target,

T = transmission of atmosphere,

L_p = path radiance, and

E = irradiance on the target.

$= (E_0 cos\theta_0)/d^2$. Here d is the earth-sun distance, θ_0 is the sun zenith angle, and E_0 is the solar irradiance at mean earth-sun distance.

Atmospheric correction

Atmospheric particles and gases will influence the transmittance of the signal through the atmosphere by absorption, and considerably change the signal. The magnitude of the water-leaving radiance is small compared to the contribution of atmospheric effects. The influence from the atmosphere must therefore be removed in order to obtain information about the water leaving radiance. The process of deriving the *normalized water-leaving radiance* -radiance that would exit the ocean in the absence of the atmosphere and with the sun at the zenith- from imagery of the oceans is usually termed *atmospheric correction* [48, Atbd-mod 17].

The normalized water-leaving radiance, $[L_w]_N$, was defined by Gordon and Clark through

$$L_w(\lambda) = [L_w(\lambda)]_N \cos\theta_0 \, exp\left[-\left(\frac{\tau_r(\lambda)}{2} + \tau_{Oz}(\lambda) \right) \left(\frac{1}{\cos\theta_0} \right) \right] \qquad (2.3.3)$$

where $L_w(\lambda)$ is the radiance backscattered out of the water at a wavelength λ, $\tau_r(\lambda)$ and $\tau_{Oz}(\lambda)$ are the optical thicknesses of the atmosphere associated with molecular (Rayleigh) scattering and Ozone absorption, respectively. Furthermore, θ_0 is the solar zenith angle.

To derive an oceanic surface temperature from the calibrated radiances at satellite height (or top-of-atmosphere brightness temperatures) it is necessary to correct for the effects of the intervening atmosphere. This is the role of the sea-surface temperature retrieval algorithm, sometimes referred to as the *atmospheric correction algorithm*.

The simplest atmospheric correction algorithm is a linear function of a single band. This has a prospect of being effective if the band is in a very clear spectral interval that is largely unaffected by water vapor. The algorithm is:

$$SST_i = a_i + b_i T_i, \qquad (2.3.4)$$

Table 2.1: Coefficients and residual SST errors of linear single band atmospheric correction algorithm [Atbd-mod25].

Band	a_1	b_1	$\varepsilon(sst)$
20	1.01342	1.04948	0.320
22	1.64547	1.02302	0.170
23	3.65264	1.04657	0.446

where i is the band number and T is the brightness temperature (i.e., the temperature of a black-body that would give the same channel radiance). The coefficients and residual SST errors are shown as Table 2.1.

The integrated atmospheric transmissivity over each of the MODIS infrared bands (20, 22, 23, 31, and 32) differs. Consequently, algorithms can be constructed which depend on the differences in measured temperature among these bands [Anding and Kauth, 1970]. Algorithm assumes that, the true surface temperature can be parameterized as a simple function of the difference between the measured temperatures in two bands with different atmospheric transmissions. They are based on a formula of the following form for the surface temperature T_s

$$T_s = \alpha + \beta T_i + \gamma T_i - T_j, \qquad (2.3.5)$$

where the coefficients α, β and γ give the parameterized correction. [Deschamps and Phulpin, 1980; Llewellyn-Jones et al., 1984]

2.3.2 Overview of MODIS Aqua Data Processing and Distribution

Level-1A Processing

Level-1A data consist of unprocessed raw data at full resolution, including radiometric and geometric calibration coefficients, computed and appended to the image data.

Level-1A is performed using the standard code developed by the MODIS *Science*

Data Support Team (SDST), known as MOD-PR01 (modis-l1agen in SeaDAS) The output of MOD-PR01 is a 5-minute Level-1A granule in HDF format. These standard Level-1A files are then reduced in the process called $MYD - L1A_SS$, where excess bands and data that are not utilized by Oceans are removed. The resulting Level-1A files are smaller in size and easier to work with. The Level-1A file format uses 16-bit integers to store the 12-bit data, so 4 bits of unused space are available. Using correlation between the high resolution land bands and the closest corresponding ocean bands, the counts stored in bands 10, 12, 13, and 16 were extended above their original 12-bit saturation limit up to the 16-bit limit of the Level-1A format.

Geolocation

The next step in the processing involves generation of the geolocation. This is performed using standard SDST code known as MOD-PR03 (geolocate in SeaDAS). For the NRT stream, the predicted attitude and ephemeris files are used to produce Quick-Look GEO files. Several days later, in the Refined processing stream, the definitive attitude and ephemeris files are used to create the final GEO version. GEO files are not maintained in the long-term archive, since they can be regenerated as needed using the much smaller attitude and ephemeris files. Therefore, only a short-term rolling archive is made available for distribution.

Level-1B

After the geolocation step, the Level-1A file and the GEO file for each 5-minute granule are fed into MYD-PR02 (aqua - l1bgen in SeaDAS) to produce the corresponding Level-1B file.The standard MYD-PR02 code is developed and maintained by the MODIS Calibration Support Team (MCST). The standard Level-1B format for 1-km data includes a pair of SDS fields for 250-meter and 500-meter that have been aggregated to 1-km.Since the Ocean Level-1A does not include the high-resolution bands, these aggregated fields would normally be unfilled.The OBPG uses this free space to store the extended ocean band information from bands 10, 12, 13lo, and 16, as these high reflectance values will not fit into the standard scaled integer fields provided for the Level-1B reflectances.

Level-2

A Level-2 data product is a processed product where a sensitivity loss correction, atmospheric correction, and chlorophyll derivation algorithm have bee applied to a level 1 product to calculate surface reflectances, land/cloud flags, subsurface reflectances, atmospheric signals, and chlorophyll concentration.

Level-2 processing is performed using the Multi-Sensor Level-1 to Level-2 (MSL12) code and generates Level-2 geophysical products by applying atmospheric corrections and bio-optical algorithms to the sensor data. The input data levels required for msll2 processing for MODIS is the Level-1B file and the GEO file. The Level-2 processing also makes use of meteorological and ozone information from ancillary sources. Figure 2.6 gives an overview of the MODIS data flow within the OBPG.
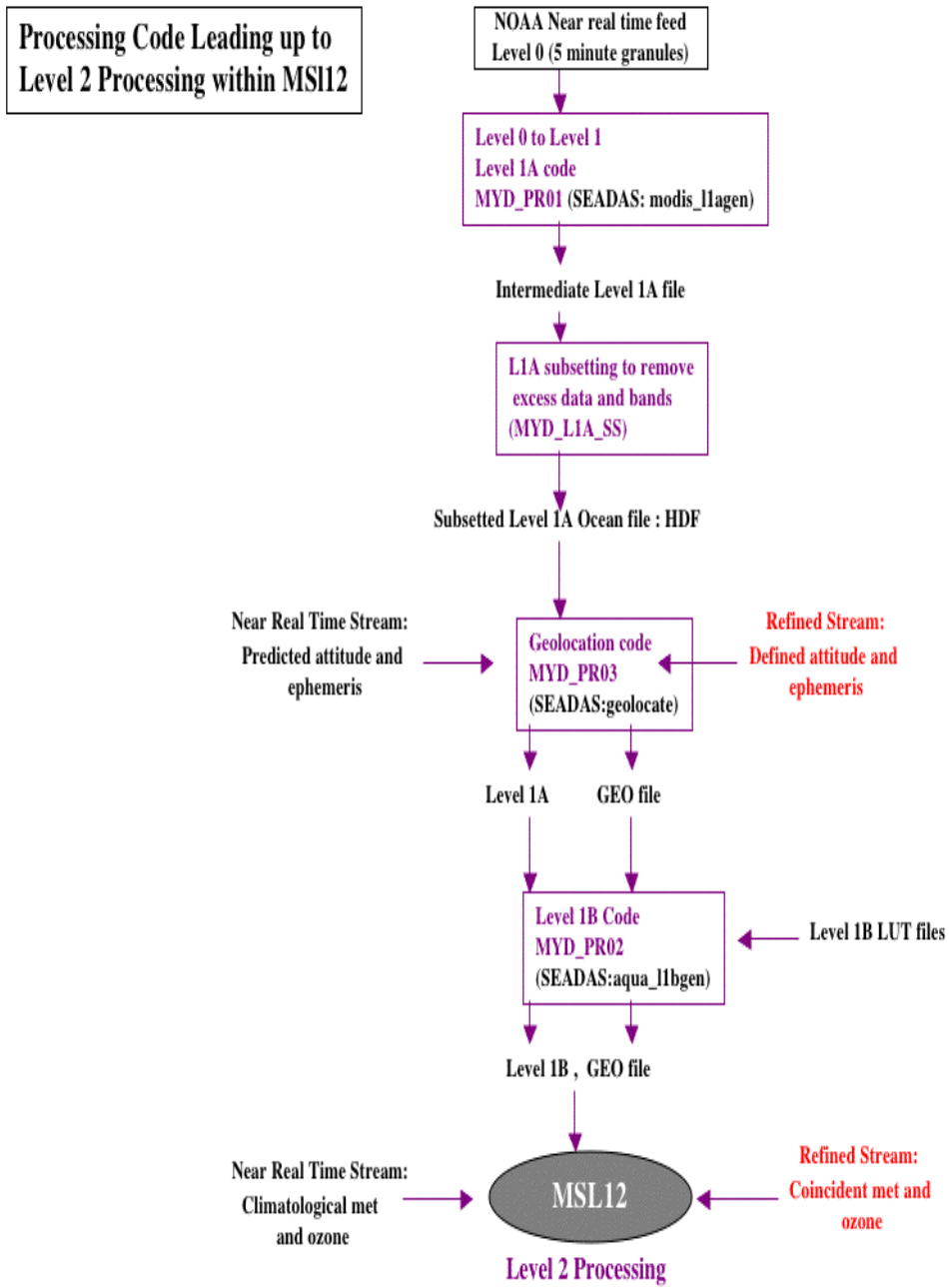
Figure 2.3: Level-2 processing.

2.3.3   Implementation of SST Processing

Short-wave SST Algorithm

The short-wave SST algorithm makes use of MODIS bands 22 and 23 at 3.959 amd 4.050 μm. The brightness temperatures are derived from the observed radiances by inversion (in log space) of a the radiance versus blackbody temperature relationship. For msl12 (Multi-Sensor Level-1 to Level-2 code), these relationships were precomputed for the spectral response of each MODIS channel, and the tables were then stored in HDF files to be loaded at run-time. In modsst, the radiance versus blackbody temperature relationship was computed at run-time. The algorithm for computing short-wave SST (sst4) from observed brightness temperatures is shown below.

$$sst4 = a_0 + a_1 BT_39 + a_2 d_{BT} + a_3(\frac{1.0}{\mu} - 1.0), \qquad (2.3.6)$$

where: $d_{BT} = BT_{39} - BT_{40}$,

BT_{39} = brightness temperature at 3.959 μm, in $^\circ C$,

BT_{40} = brightness temperature at 4.050 μm, in $^\circ C$,

μ = cosine of sensor zenith angle.

The coefficients a_0, a_1, a_2, and a_3 are derived and continuously verified by RSMAS based on match-ups between the satellite retrievals of brightness temperature and field measurements of sea surface temperature. As currently implemented, these coefficients can be time-dependent. The coefficients are provided to msl12 through external files, which are in a columnated ascii format of "sensor start-date end-date a_0 a_1 a_2 a_3".

The short-wave infrared bands near $4\mu m$ are affected by bright reflective sources such as sun glint. Due to such contamination, the short-wave SST product is not considered valid for daytime use.

Long-wave SST Algorithm

The long-wave SST algorithm makes use of MODIS bands 31 and 32 at 11 amd 12 μm. The brightness temperatures are derived from the observed radiances by inversion (in linear space) of the radiance versus blackbody temperature relationship. For msl12, these relationships were precomputed for the spectral response of each MODIS channel, and the tables were then stored in HDF files to be loaded at run-time. In modsst, the radiance versus blackbody temperature relationship was computed at run-time. The nonlinear SST algorithm was tuned for two different regimes based on brightness temperature difference. The algorithm for computing long-wave SST from observed brightness temperatures is shown below:

$$d_{BT} \leq 0.5,$$

$$sst = a_{00} + a_{01}BT_{11} + a_{02}d_{BT}bsst + a_{03}d_{BT}(\frac{1.0}{\mu} - 1.0),$$

$$d_{BT} \geq 0.9,$$

$$sst = a_{10} + a_{11}BT_{11} + a_{12}d_{BT}bsst + a_{13}d_{BT}(\frac{1.0}{\mu} - 1.0),$$

$$0.5 < d_{BT} < 0.9,$$

$$sst_{lo} = a_{00} + a_{01}BT_{11} + a_{02}d_{BT}bsst + a_{03}d_{BT}(\frac{1.0}{\mu} - 1.0),$$

$$sst_{hi} = a_{10} + a_{11}BT_{11} + a_{12}d_{BT}bsst + a_{13}d_{BT}(\frac{1.0}{\mu} - 1.0),$$

$$sst = sst_{lo} + \frac{d_{BT} - 0.5}{0.9 - 0.5}(sst_{hi} - sst_{lo}),$$

where: $d_{BT} = BT_{11} - BT_{12}$,

BT_{11} = brightness temperature at 11 μm in °C,

BT_{12} = brightness temperature at 12 μm, in °C,

$b_s st$ = baseline SST, which is either sst4 (if valid) or sst_{ref} (from oi_{sst}),

μ = cosine of sensor zenith angle.

At night, where sst4 retrieval is reliable, the algorithm uses sst4 for the bsst value. For daytime SST, the algorithm uses a reference SST source (sstref) for bsst, where sstref is operationally derived from the weekly Reynolds oisst product, bilinearly interpolated to the pixel location. The coefficients a_{00}, a_{01} , a_{02},a_{03} and a_{10}, a_{11}, a_{12}, and a_{13} are derived and continuously verified by RSMAS based on match-ups between the satellite retrievals of brightness temperature and field measurements of sea surface temperature.

MODIS homepage:
http://oceancolor.gsfc.nasa.gov/DOCS/modis_sst/sst_modisa.dat

2.3.4 MODIS ocean data processing codes

The main aim of the MODIS ocean processing code is to calculate level 2, 3, and 4 ocean products from level 1B satellite radiance data. This process is performed in several stages, where the ocean color and sea-surface temperature (SST) level 2 products are first calculated, followed by space and time-binning to retrieve level 3 products, and statistical mapping to yield level 4 products.

The ocean color processing routine (MODCOL) includes atmospheric correction algorithms to convert level 1B radiances to water-leaving radiances, as well as algorithms to derive level 2 ocean color products such as chlorophyll concentration.

The code is divided into six main components:

 MODCOL : performs atmospheric correction and applies the ocean color algorithms to level 1B data,

MODSST : calculates the sea-surface temperature (SST) from level 1B data,

MSBIN : space bins the level 2 data,

MTBIN : time bins the level 2 data,

MFILL : calculates a 24-day reference,

MCLOUD : declouds the data,

and two auxiliary components:

MMAP : maps data onto geographic projections,

MSPC : changes the spatial resolution of the binned data.

We only pay attention to MODCOL and MODSST applied to our level 2 data to improve accuracy. Level 1B data, geolocation data, ancillary data, cloud mask data, aerosol data, water vapor data (SST calculations only) and 24-day SST reference data (SST calculations only), are input into MODCOL and MODSST.

MODCOL

This program processes level 1B data, creating level 2 ocean color data products. The program first applies atmospheric correction to the level 1B data, and then estimates a suite of ocean color products using a number of ocean color algorithms.

Level 1B satellite data, geolocation data, cloud mask data and aerosol data are obtained from the satellite data itself. Ancillary data (algorithm coefficients, meteorology, ozone, etc.) are obtained from external files.

MODSST

This program calculates level 2 sea-surface temperature (SST) products from level 1B satellite data. It calls the main subroutine modsstmain which calls the remaining subroutines.

The input files required for processing of SST data are:

level 1B satellite data,

geolocation data,

cloud mask data,

aerosol data,

water vapor,

24-day SST reference OR Reynolds SST data (currently used),

ancillary data (algorithm coefficients, meteorology, ozone, etc.).

The first five files are obtained from the satellite data itself.

Each of these programs outputs -in hdf file- contain the indicated ocean color products as well as metadata. Metadata contain auxiliary information such as the creation date, datatime, principal investigator, sensor characteristics, algorithms used, etc. [$http://modis.gsfc.nasa.gov/data/algorithms.html$].

Full documentation, updated code source, sensor files, and output product descriptions can be found at http://oceancolor.gsfc.nasa.gov/DOCS and MODIS home page

In this study, SST-night ($4\mu m$) and sst-day ($12\mu m$) MODIS Aqua data were used. Before using these hdf (hierachical data format) type data we use several techniques to gain meaningful form of SST, quality level, l2-flags, latitude and longitude. (See Appendix A for *converthdf.m.*)

CHAPTER 3

MATHEMATICAL BACKGROUND

3.1 Introduction to Vectors and Matrices

A real $N-$dimensional vector X is an ordered set of N real numbers and is usually written in the coordinate form

$$X = (x_1, x_2, \ldots, x_N).$$

Here the numbers $x_1, x_2, \ldots,$ and x_N are called the *components of X*. The set consisting of all $N-$ dimensional vectors is called $N - dimensional\ space$. When a vector is used to denote a point or position in space, it is called *position vector*. When it is used to denote a movement between two points in space, it is called a *displacement vector*.

Let another vector be $Y = (y_1, y_2, \ldots, y_N)$. The two vectors X and Y are said to be equal if and only if each corresponding coordinate is the same.

The sum of the vectors X and Y is computed component by component.

The negative of the vector X is obtained by replacing each coordinate with its negative.

The difference $Y - X$ is formed by taking the difference in each coordinate.

Vectors in N-dimensional space obey the algebraic property

$$Y - X = Y + (-X).$$

If c is a real number (scalar), we define scalar multiplication cX as follows:

$$cX = (cx_1, cx_2, \ldots, cx_N).$$

If c and d are scalars, then the weighted sum $cX + dY$ is called a linear combination of X and Y and we write

$$cX + dY = (cx_1 + dy_1, cx_2 + dy_2, \ldots, cx_N + dy_N).$$

The dot product of the two vectors X and Y is a scalar quantity (real number) defined by the equation

$$X \cdot Y = x_1 y_1 + x_2 y_2 + \ldots + x_N y_N.$$

The norm (or length) of the vector X is defined by

$$\|X\| = \sqrt{x_1^2 + x_2^2 + \ldots + x_N^2}.$$

An important relationship exists between the dot product and norm of a vector. Using last two equations we have

$$\|X\|^2 = x_1^2 + x_2^2 + \ldots + x_N^2 = X \cdot X.$$

The formula for the distance between two points in N-space is

$$\|Y - X\| = \sqrt{(y_1 - x_1)^2 + (y_2 - x_2)^2 + \ldots + (y_N - x_N)^2}.$$

3.1.1 Matrices and Two-dimensional Arrays

A matrix is a rectangular array of numbers that is arranged systematically in rows and columns. A matrix having M rows and N columns is called an $M \times N$ (read "M by N") matrix. The capital letter A denotes a matrix, and the lowercase subscripted letter a_{ij} denotes one of the numbers forming the matrix. We write

$$A = [a_{ij}]_{M \mathbf{x} N}.$$

We refer to a_{ij} as the entry in location (i, j).

The rows of the $M \times N$ matrix A are $N-$dimensional vectors:

$$V_i = (a_{i1}, a_{i2}, \ldots, a_{iN}) \quad \text{for} \quad i = 1, 2, \ldots, M.$$

In expanded form we write

$$
\begin{bmatrix}
a_{11} & a_{12} & \ldots & a_{1j} & \ldots & a_{1N} \\
a_{21} & a_{22} & \ldots & a_{2j} & \ldots & a_{2N} \\
\vdots & \vdots & & \vdots & & \vdots \\
a_{i1} & a_{i2} & \ldots & a_{ij} & \ldots & a_{iN} \\
\vdots & \vdots & & \vdots & & \vdots \\
a_{M1} & a_{M2} & \ldots & a_{Mj} & \ldots & a_{MN}
\end{bmatrix} = A
$$

Let $A = [a_{ij}]_{M \times N}$ and $B = [b_{ij}]_{M \times N}$ be two matrices of the same dimension. The two matrices A and B are said lo be equal if and only if each corresponding element is the same; that is,

$$A = B \quad \text{if and only if} \quad a_{ij} = b_{ij} \quad \text{for } 1 \leq i \leq M, \ 1 \leq j \leq N.$$

The sum of the two $M \times N$ matrices A and B is computed element by element,

using the definition

$$A + B = [a_{ij} + b_{ij}]_{M \times N} \quad \text{for } 1 \le i \le M, \ 1 \le j \le N.$$

The negative of the matrix A is obtained by replacing each element with its negative:

$$-A = [-a_{ij}]_{M \times N} \quad \text{for } 1 \le i \le M, \ 1 \le j \le N.$$

The difference AB is formed by taking the difference of corresponding coordinates:

$$A - B = [a_{ij} - b_{ij}]_{M \times N} \quad \text{for } 1 \le i \le M, \ 1 \le j \le N.$$

If c is a real number (scalar), we define scalar multiplication cA as follows:

$$cA = [ca_{ij}]_{M \times N} \quad \text{for } 1 \le i \le M, \ 1 \le j \le N.$$

If p and q are scalars, the weighted sum $pA + qB$ is called a linear combination of the matrices A and B, and we write

$$pA + qB = [pa_{ij} + qb_{ij}]_{M \times N} \quad \text{for } 1 \le i \le M, \ 1 \le j \le N.$$

3.1.2 Properties of Vectors and Matrices

A linear combination of the variables $x_1, x_2, \ldots, x_N$ is a sum

$$a_1 x_1 + a_2 x_2 + \ldots + a_N x_N,$$

where a_k is the coefficient of x_k for $k = 1, 2, \ldots, N$.

A linear equation in $x_1, x_2, \ldots, x_N$ is obtained by requiring the linear combination

in the previous equation to take on a prescribed value b; that is,

$$a_1 x_1 + a_2 x_2 + \ldots + a_N x_N = b.$$

Systems of linear equations arise frequently, and if M equations in N unknowns are given, we write

$$
\begin{aligned}
a_{11} x_1 &+ a_{12} x_2 + \ldots + a_{1N} x_N &= b_1 \\
a_{21} x_1 &+ a_{22} x_2 + \ldots + a_{2N} x_N &= b_2 \\
&\vdots \qquad \vdots \qquad\qquad \vdots \qquad\quad \vdots \\
a_{k1} x_1 &+ a_{k2} x_2 + \ldots + a_{kN} x_N &= b_k \\
&\vdots \qquad \vdots \qquad\qquad \vdots \qquad\quad \vdots \\
a_{M1} x_1 &+ a_{M2} x_2 + \ldots + a_{MN} x_N &= b_M
\end{aligned}
$$

A solution to this is a set of numerical values $x_1, x_2, \ldots, x_N$ that satisfies all the equations in simultaneously. Hence a solution can be viewed as an $N-$dimensional vector;

$$X = (x_1, x_2, \ldots, x_N).$$

We now discuss how to use matrices to represent a linear system of equations. The linear equations above can be written as a matrix product. The coefficients a_{kj} are stored in a matrix A (called the *coefficient matrix*) of dimension $M \times N$, and the unknowns x_j are stored in a matrix X of dimension $N \times 1$, The constants b_k are stored in a matrix B of dimension $M \times 1$. It is conventional to use column

matrices for both X and B and we write

$$AX = \begin{bmatrix} a_{11} & a_{12} & \dots & a_{1j} & \dots & a_{1N} \\ a_{21} & a_{22} & \dots & a_{2j} & \dots & a_{2N} \\ \vdots & \vdots & & \vdots & & \vdots \\ a_{k1} & a_{k2} & \dots & a_{kj} & \dots & a_{kN} \\ \vdots & \vdots & & \vdots & & \vdots \\ a_{M1} & a_{M2} & \dots & a_{Mj} & \dots & a_{MN} \end{bmatrix} \begin{bmatrix} x_1 \\ x_2 \\ \vdots \\ x_j \\ \vdots \\ x_N \end{bmatrix} = \begin{bmatrix} b_1 \\ b_2 \\ \vdots \\ b_j \\ \vdots \\ b_M \end{bmatrix} = B.$$

The matrix multiplication $AX = B$ is reminiscent of the dot product for ordinary vectors, because each element b_k in B is the result obtained by taking the dot product of row k in matrix A with the column matrix X.

3.1.3   Solutions to Systems of Linear Equations

The following is an example of a system of three linear equations with three unknowns (x_1, x_2, x_3):

$$\begin{aligned} 3x_1 & +2x_2 & -x_3 & =10 \\ -x_1 & +3x_2 & +2x_3 & =5 \\ x_1 & -x_2 & -x_3 & =-1 \end{aligned}$$

This system of equations can be rewritten in matrix form as

$$Ax = \begin{bmatrix} 3 & 2 & -1 \\ -1 & 3 & 2 \\ 1 & -1 & -1 \end{bmatrix} \begin{bmatrix} x_1 \\ x_2 \\ x_3 \end{bmatrix} = \begin{bmatrix} 10 \\ 5 \\ -1 \end{bmatrix} = B.$$

The system of equations is nonsingular if the matrix A containing the coefficients of the equations is nonsingular. The rank of A must be equal to the number of rows of A and the determinant $|A|$ must be nonzero for the system of equations to be nonsingular.

Solution by Matrix Inverse

Premultiply the system of equations $Ax = b$ by A^{-1}

$$A^{-1}Ax = A^{-1}b.$$

Because $A^{-1}A$ is equal to the identity matrix I [19]

$$Ix = A{-}1b \quad \text{or} \quad x = A^{-1}b.$$

We can use this method if A is a square matrix. If A is not square, a $M \times N$ matrix *pseudoinverse* operator A^{+} may be used to determine a solution.

Pseudoinverse Operators

The first type of pseudoinverse operator to be introduced is the generalized inverse A^{-}, which satisfies the following relations [14]:

$$AA^{-} = [AA^{-}]^{T},$$
$$A^{-}A = [A^{-}A]^{T},$$
$$AA^{-}A = A,$$
$$A^{-}AA^{-} = A^{-}.$$

The generalized inverse is unique. It may be expressed explicitly under certain circumstances. If $M > N$, the system is said to be *overdetermined*; that is, there are more observations than points to be estimated. In this case, if A is of rank N, the generalized inverse may be expressed as

$$A^{-} = [A^{T}A]^{-1}A^{T}.$$

At the other extreme, if $M < N$ the system is said to be *underdetermined*. In this case, if A is of rank M, the generalized inverse is equal to

$$A^{-} = A^{T}[A^{T}A]^{-1}.$$

Another type of pseudoinverse operator is the least-squares inverse $A^\S$, which satisfies the defining relations

$$AA^\S A = A,$$
$$AA^\S = [AA^\S]^T.$$

Finally, a conditional inverse $A^\sharp$ is defined by the relation

$$AA^\sharp A = A.$$

Examination of the defining relations for the three types of pseudoinverse operators reveals that the generalized inverse is also a least-squares inverse, which in turn is also a conditional inverse. Least-squares and conditional inverses exist for a given linear operator A; however, they may not be unique. Furthermore, it is usually not possible to explicitly express these operators in closed form. The following is a list of useful relationships for the generalized inverse operator of a $M \times N$ matrix A [8].

3.1.4   Singular Value Matrix Decomposition (SVD)

Any arbitrary $M \times N$ matrix A of rank R can be decomposed into the sum of a weighted set of unit rank $M \times N$ matrices by a singular-value decomposition (SVD).

According to the SVD matrix decomposition, there exist an $M \times M$ unitary matrix U and an $N \times N$ unitary matrix V for which

$$U^T A V = \Lambda^{1/2}$$

where

$$\Lambda^{1/2} = \begin{bmatrix} \lambda^{1/2}(1) & \dots & & 0 \\ \vdots & \ddots & & \vdots \\ & & \lambda^{1/2}(1) & \\ 0 & \dots & & 0 \end{bmatrix}$$

is an $M \times N$ matrix with a general diagonal entry $\lambda^{1/2}(j)$ called a *singular value* of A. Since U and V are unitary matrices, $UU^T = I_M$ and $VV^T = I_N$. Consequently,

$$A = U\Lambda^{1/2}V^T.$$

3.2   Interpolation and Curve Fitting

The very processes of interpolation and curve fitting are basically attempts to get "something for nothing". In general, one has a function defined at a discrete set of points and desires information about the function at some other point. Well that information simply does not exist. One must make some assumptions about the behavior of the function. This is where some of the "art of computing" enters the picture. One needs some knowledge of what the discrete entries of the table represent. In picking an interpolation scheme to generate the missing information, one makes some assumptions concerning the functional nature of the tabular entries. That assumption is that they behave as polynomials. All interpolation theory is based on polynomial approximation [19, 21].

Precisely, given $n + 1$ pairs $(t_k, x(t_k))$, the problem consists of finding a function $p = p(t)$ such that $p(t_k) = x(t_k)$ for $i = 0, \dots, m$, $x(t_k)$ being some given values, and say that p interpolates $x(t_k)$ at the nodes t_k. We speak about polynomial interpolation if p is an algebraic polynomial, trigonometric approximation if p is a trigonometric polynomial or piecewise polynomial interpolation (or spline interpolation) if p is only locally a polynomial [14].

The problem of finding $\hat{x}(t, \alpha)$ -to minimize the error

$$e(t_k) = x(t_k) - \hat{x}(t_k, \alpha) \qquad , (k \in \mathbb{Z}_{n+1}), \qquad (3.2.1)$$

where α is the vector of unknown parameters- is often called *curve fitting*. Curve fitting is used when the data are uncertain because of the corrupting effects of measurement errors, random noise, or interference. Interpolation is appropriate when the data are accurately or exactly known.

Interpolation is quite important in processing. For example, bandlimited signals may need to be interpolated in order to change sampling rates. Interpolation is vital in numerical integration methods, as will be seen later. In this application the integrand is typically known or can be readily found at some finite set of points with significant accuracy. Interpolation at these points leads to a function (usually a polynomial) that can be easily integrated, and so provides a useful approximation to the given integral.

3.2.1 Lagrange Interpolation

Assume that we wish to interpolate the data set $\{(t_k, x_k)|k \in \mathbb{Z}_{n+1}\}$. Suppose that we possess polynomials (called *Lagrange polynomials*) $L_j(t)$ with the property

$$L_j(t_k); = \begin{pmatrix} 0 & , & j \neq k \\ 1 & , & j = k \end{pmatrix} = \delta_{j-k}. \qquad (3.2.2)$$

Then the interpolating polynomial for the data set is

$$p_n(t) = x_0 L_0(t) + x_1 L_1(t) + \ldots + x_n L_n(t) = \sum_{j=0}^{n} x_j L_j(t). \qquad (3.2.3)$$

We observe that

$$p_n(t_k) = \sum_{j=0}^{n} x_j L_j(t_k) = \sum_{j=0}^{n} x_j \delta_{j-k} = x_k \qquad (3.2.4)$$

for $k \in \mathbb{Z}_{n+1}$ so $p_n(t)$ in (3.2.6) does indeed interpolate the data set. We may see that for $j \in \mathbb{Z}_{n+1}$ the Lagrange polynomials are given by

$$L_j(t) = \prod_{i=0}^{n} \frac{t - t_i}{t_j - t_i}, \qquad i \neq j. \tag{3.2.5}$$

Equation (3.2.6) is called the *Lagrange form of the interpolating polynomial* [37].

3.2.2   Newton Interpolation

Define
$$x[t_0.t_1] = \frac{x(t_1) - x(t_0)}{t_1 - t_0} = \frac{x_1 - x_0}{t_1 - t_0}. \tag{3.2.6}$$

This is called the *first divided difference of $x(t)$ relative to t_1 and t_0*. We see that $x[t_0, t_1] = x[t_1, t_0]$. We may linearly interpolate $x(t)$ for $t \in [t_0, t_1]$ according to

$$x(t) \approx x(t_0) + \frac{t - t_0}{t_1 - t_0}[x(t_1) - x(t_0)] = x(t_0) + (t - t_0)x[t_0, t_1]. \tag{3.2.7}$$

It is convenient to define $p_0(t) = x(t_0)$ and $p_1(t) = x(t_0) + t - t_0 x[t_0, t_1]$ (it is consistent with previous section). In fact, $p_1(t)$ agrees with the solution to

$$\begin{bmatrix} 1 & t_0 \\ 1 & t_1 \end{bmatrix} \begin{bmatrix} p_{1,0} \\ p_{1,1} \end{bmatrix} = \begin{bmatrix} x_0 \\ x_1 \end{bmatrix} \tag{3.2.8}$$

as we expect.

Unless $x(t)$ is truly linear the secant slope $x[t_0, t_1]$ will depend on the abscissas t_0 and t_1 If x_t is a second degree polynomial then $x[t1, t]$ will itself be a linear function of t for a given t_1. Consequently, the ratio

$$x[t_0, t_1, t_2] = \frac{x[t_1, t_2] - x[t_0, t_1]}{t_2 - t_0} \tag{3.2.9}$$

will be independent of t_0, t_1, and t_2. (This ratio is the second divided difference of $x(t)$ with respect to t_0, t_1, and t_2.)

$$x(t) \approx x(t_0) + (t - t_0)x[t_0, t_1] + (t - t_0)(t - t_1)x[t_0, t_1, t_2] = p_2(t) \qquad (3.2.10)$$

is the *second-degree interpolation formula*, while (3.2.10) is the *first-degree interpolation formula*.

Continuing in this fashion, we obtain

$$x(t) = x[t_0] + (t - t_0)x[t_0, t_1] + (t - t_0)(t - t_1)x[t_0, t_1, t_2] + \ldots$$

$$+(t - t_0)(t - t_1) \ldots (t - t_{n-1})x[t_0, t_1, \ldots, t_n] + e(t), \qquad (3.2.11)$$

where
$$e(t) = (t - t_0)(t - t_1) \ldots (t - t_n)x[t_0, t_1, \ldots, t_n, t], \qquad (3.2.12)$$

and we define

$$p_n(t) = x[t_0] + (t - t_0)x[t_0, t_1] + (t - t_0)(t - t_1)x[t_0, t_1, t_2] + \ldots$$

$$+(t - t_0) \ldots (t - t_{n-1})x[t_0, \ldots, t_n], \qquad (3.2.13)$$

which is the *nth-degree interpolating formula*, and is clearly a polynomial of degree n. So $e(t)$ is the error involved in interpolating $x(t)$ using polynomial $p_n(t)$. Equation (3.2.11) is the *Newton interpolating formula with divided differences*.If $x(t)$ is a polynomial of degree n (or less), then $e(t) = 0$ (for all t).

3.2.3 Spline Interpolation

Splines are interpolative polynomials that involve information concerning the derivative of the function at certain points. Unlike Hermite interpolation that explicitly invokes knowledge of the derivative, splines utilize that information implicitly so that specific knowledge of the derivative in not required. Unlike general interpolation formulae of the Lagrangian type, which maybe used in a

small section of a table, splines are constructed to fit an entire run of tabular entries of the independent variable. While one can construct splines of any order, the most common ones are cubic splines as they generate tri-diagonal equations for the coefficients of the polynomials [8, 21]. Chapter 5 includes details of spline interpolation.

Speed, **Memory**, **and Smoothness Considerations**

When choosing an interpolation method, we should keep in mind that some require more memory or longer computation time than others.

Nearest neighbor interpolation is the fastest method. However, it provides the worst results in terms of smoothness. This method sets the value of an interpolated point to the value of the nearest data point. Therefore, this method does not generate any new data points.

Linear interpolation uses more memory than the nearest neighbor method, and requires slightly more execution time. Unlike nearest neighbor interpolation its results are continuous, but the slope changes at the vertex points.

Cubic spline interpolation has the longest relative execution time, although it requires less memory than cubic interpolation. It produces the smoothest results of all the interpolation methods. You may obtain unexpected results, however, if your input data is non-uniform and some points are much closer together than others.

Cubic interpolation requires more memory and execution time than either the nearest neighbor or linear methods. However, both the interpolated data and its derivative are continuous [10, 11].

3.3   Mathematical Morphology

The field of mathematical morphology contributes a wide range of operators to image processing, all based around a few simple mathematical concepts from

set theory. The operators are particularly useful for the analysis of binary images and common usages include edge detection, noise removal, image enhancement and image segmentation.

The two most basic operations in mathematical morphology are erosion and dilation. Both of these operators take two pieces of data as input: an image to be eroded or dilated, and a structuring element (also known as a kernel). The two pieces of input data are each treated as representing sets of coordinates in a way that is slightly different for binary and grayscale images [45].

Erosion and dilation work (at least conceptually) by translating the structuring element to various points in the input image, and examining the intersection between the translated kernel coordinates and the input image coordinates. Virtually all other mathematical morphology operators can be defined in terms of combinations of erosion and dilation along with set operators such as intersection and union. Some of the more important are opening, closing and skeletonization.

3.3.1   Dilation

Dilation is one of the two basic operators in the area of mathematical morphology, the other being erosion. It is typically applied to binary images, but there are versions that work on grayscale images. The basic effect of the operator on a binary image is to gradually enlarge the boundaries of regions of foreground pixels (i.e., white pixels, typically). Thus areas of foreground pixels grow in size while holes within those regions become smaller.

The dilation operator takes two pieces of data as inputs. The first (A) is the image which is to be dilated. The second (B) is a (usually small) set of coordinate points known as a structuring element (also known as a *kernel*). It is this structuring element that determines the precise effect of the dilation on the input image.

The techniques of morphological filtering can be extended to gray-level images. To simplify matters we will restrict our presentation to structuring elements that

comprise a finite number of pixels and are convex and bounded. Now, however, the structuring element has gray values associated with every coordinate position as does the image A [11, 45].

$$D(A, B) := \max_{[j,k] \in B} a[m - j, n - k] + b[j, k]. \qquad (3.3.14)$$

For a given output coordinate $[m, n]$, the structuring element is summed with a shifted version of the image and the maximum encountered over all shifts within the $J \times K$ domain of B is used as the result.

3.3.2 Erosion

The basic effect of the operator on a binary image is to erode away the boundaries of regions of foreground pixels (i.e., white pixels, typically). Thus areas of foreground pixels shrink in size, and holes within those areas become larger:

$$E(A, B) := \min_{[j,k] \in B} a[m + j, n + k] + b[j, k]. \qquad (3.3.15)$$

For a given output coordinate $[m, n]$, the structuring element is summed with a shifted version of the image and the maximum encountered over all shifts within the J x K domain of B is used as the result [45].

3.3.3 Opening and closing

Opening and closing are two important operators from mathematical morphology. They are both derived from the fundamental operations of erosion and dilation. The basic effect of an opening is somewhat like erosion in that it tends to remove some of the foreground (bright) pixels from the edges of regions of foreground pixels. However, it is less destructive than erosion in general. Closing

is similar in some ways to dilation in that it tends to enlarge the boundaries of foreground (bright) regions in an image (and shrink background color holes in such regions), but it is less destructive of the original boundary shape. Closing is the dual of opening, i.e., closing the foreground pixels with a particular structuring element, is equivalent to closing the background with the same element [11].

CHAPTER 4

INTRODUCTION TO IMAGE PROCESSING

In this chapter we will briefly summarize digital image processing techniques for edge detection, segmentation and reconstruction. Detailed methods used or compared in this thesis can be found in Chapter 5.

4.1 Edge Detection

Edges are areas in an image where rapid changes occur in the intensity function or in spatial derivatives of this intensity function which could be due to discontinuities in scene reflectance, surface orientation, or depth [16]. Image pixels representing such discontinuities carry more information than pixels representing gradual change or no change in intensities.

The base of edge detection is differentiation. Note that the detected edge is the derivative of the edge. This means it is the slope or rate of change of the gray levels in the edge. The slope of the edge is always positive or zero, and it reaches its maximum at the edge. For this reason, edge detection is often called *image differentiation*.

The gradient of an image f at location (x, y), along the line normal to the edge slope, is the vector

$$\nabla f = \left[\begin{array}{c} f_x \\ f_y \end{array} \right] = \left[\begin{array}{c} \frac{\partial f}{\partial x} \\ \frac{\partial f}{\partial y} \end{array} \right]. \tag{4.1.1}$$

The spatial gradient amplitude is given by:

$$G(x, y) = \sqrt{f_x^2 + f_y^2} \tag{4.1.2}$$

and the gradient direction with respect to the row axis is

$$\Theta(x, y) = \arctan \frac{f_y}{f_x}. \tag{4.1.3}$$

The first order derivative edge detection can be carried out either by using two orthogonal directions in an image or by using a set of directional derivatives.

Thresholding and thinning : The most commonly used method of producing edge segments or contours from (4.1.2) consists of two stages: *thresholding* and *thinning*. In the thresholding stage, the gradient magnitude at every point is compared to a predefined threshold value, T. All points satisfying the following criterion are classified as candidate edge points:

$$|\nabla f(x, y)| \geq T.$$

The set of candidate edge points tends to form strips, which have positive width. Since the desire is usually for zero-width boundary segments or contours to describe the edges, a subsequent processing stage is needed to thin the strips to the final edge contours. Edge contours derived from continuous-space images should have zero width because any local maxima of $|\nabla f(x, y)|$, along a line segment that crosses the edge, cannot be adjacent points.

46

The selection of the threshold value T is a tradeoff between the wish to fully capture the actual edges in the image and the desire to reject noise. Increasing T decreases sensitivity to noise at the cost of rejecting the weakest edges, forcing the edge segments to become more broken and fragmented. By decreasing T, one can obtain more connected and richer edge contours, but the greater noise sensitivity is likely to produce more false edges.

Edge thinning can be accomplished in a number of ways, depending on the application, but thinning by nonmaximum suppression is usually the best choice. Generally speaking, we wish to suppress any point that is not, in a 1-D sense, a local maximum in gradient magnitude. Since a $1 - D$ local neighborhood search typically produces a single maximum, those points that are local maxima will form edge segments only one point wide. One approach classifies an edge-strip point as an edge point if its gradient magnitude is a local maximum in at least one direction. However, this thinning method sometimes has the side effect of creating false edges near strong edge lines. It is also somewhat inefficient because of the computation required to check along a number of different directions. A better, more efficient thinning approach checks only a single direction, the gradient direction, to test whether a given point is a local maximum in gradient magnitude. The points that pass this scrutiny are classified as edge points. The method is efficient because it is not necessary to search in multiple directions. It also tends to produces edge segments having good localization accuracy. These characteristics make the gradient direction, local extremum method quite popular. The following steps summarize its implementation.

1. Compute ∇f for all pixels.

2. Determine candidate edge pixels by thresholding all pixels gradient magnitudes by T.

3. Thin by checking whether each candidate edge pixels gradient magnitude is a local maximum along its gradient direction. If so, classify it as an edge pixel [51].

Table 4.1: Gradient edge detector masks.

Operator	H_x	H_y
Pixel difference	$\begin{bmatrix} 0 & 0 & 0 \\ 0 & 1 & -1 \\ 0 & 0 & 0 \end{bmatrix}$	$\begin{bmatrix} 0 & -1 & 0 \\ 0 & 1 & 0 \\ 0 & 0 & 0 \end{bmatrix}$
Separated pixel difference	$\begin{bmatrix} 0 & 0 & 0 \\ 1 & 0 & -1 \\ 0 & 0 & 0 \end{bmatrix}$	$\begin{bmatrix} 0 & -1 & 0 \\ 0 & 0 & 0 \\ 0 & 1 & 0 \end{bmatrix}$
Roberts	$\begin{bmatrix} 0 & 0 & -1 \\ 0 & 1 & 0 \\ 0 & 0 & 0 \end{bmatrix}$	$\begin{bmatrix} -1 & 0 & 0 \\ 0 & 1 & 0 \\ 0 & 0 & 0 \end{bmatrix}$
Prewitt	$\frac{1}{3}\begin{bmatrix} 1 & 0 & -1 \\ 1 & 0 & -1 \\ 1 & 0 & -1 \end{bmatrix}$	$\frac{1}{3}\begin{bmatrix} -1 & -1 & -1 \\ 0 & 0 & 0 \\ 1 & 1 & 1 \end{bmatrix}$
Sobel	$\frac{1}{4}\begin{bmatrix} 1 & 0 & -1 \\ 2 & 0 & -2 \\ 1 & 0 & -1 \end{bmatrix}$	$\frac{1}{4}\begin{bmatrix} -1 & -2 & -1 \\ 0 & 0 & 0 \\ 1 & 2 & 1 \end{bmatrix}$
Fei-Chen	$\frac{1}{2+\sqrt{2}}\begin{bmatrix} 1 & 0 & -1 \\ \sqrt{2} & 0 & -\sqrt{2} \\ 1 & 0 & -1 \end{bmatrix}$	$\frac{1}{2+\sqrt{2}}\begin{bmatrix} -1 & -\sqrt{2} & -1 \\ 0 & 0 & 0 \\ 1 & \sqrt{2} & 1 \end{bmatrix}$

Gradient mask operators : Gradient estimates can be obtained by using gradient operators of the form:

$$f_x = f * H_x$$
$$f_y = f * H_y$$

(4.1.4)

where $*$ denotes convolution, and H_x and H_y are 3×3 row and column operators, called gradient masks.

Pixel difference is the simplest one, which consists just of forming the difference of pixels along rows and columns of the image:

$$f_x(x_m, y_n) = f(x_m, y_n) - f(x_m - 1, y_n)$$
$$f_x(x_m, y_n) = f(x_m, y_n) - f(x_m - 1, y_n)$$

(4.1.5)

The *Roberts gradient masks* (Roberts, 1965) are more sensitive to diagonal edges. Using these masks, the orientation must be calculated by

$$\Theta(x_m, y_n) = \frac{\pi}{4} + \arctan \frac{f_y(x_m, y_n)}{f(x_m, y_n)}$$

(4.1.6)

Prewitt (1970), Sobel, and Frei-Chen (1977) produce better results than the pixel difference, separated pixel difference and Roberts operator, because the mask is larger, and provides averaging of small luminance fluctuations. The Prewitt operator is more sensitive to horizontal and vertical edges than diagonal edges, and the reverse is true for the Sobel operator. However, Sobel's operator is often a better choice than Prewitt's because the low-pass filter produced by the [1 2 1] kernel results in a smoother frequency response compared to that of [1 1 1]. The Frei-Chen edge detector has the same sensitivity for diagonal, vertical, and horizontal edges. However, even the Frei-Chen operator retains some directional sensitivity in gradient magnitude, so it is not truly isotropic. The residual anisotropy is caused by the fact that the difference operators used to approximate the gradient are not rotationally symmetric [17].

Compass operators : Compass operators measure gradients in a selected number of directions. The directions are $\Theta_k = k\frac{\pi}{4}, \quad k = 0, \ldots, 7$. The edge template

gradient is defined as:

$$G(x_m, y_n) = \max_{k=0}^{7} |f(x_m, y_n) * H_k(x_m, y_n)|. \qquad (4.1.7)$$

The Kirsch, Prewitt, and Sobel masks are *compass gradient* or directional edge detectors. Given a pixel, there are eight directions to travel to a neighboring pixel (above, below, left, right, upper left, upper right, lower left, and lower right). This means that each of the eight masks detects an edge in one direction. Therefore, there are eight possible directions for an edge. The directional edge detectors can detect an edge in only one of the eight directions. To detect only left to right edges, use only one of the eight masks. To detect all of the edges, perform convolution over an image eight times using each of the eight masks [18].

Derivative of Gaussian :

The previous methods are relatively sensitive to the noise. A solution could be to extend the window size of the gradient mask operators. Another approach is to use the derivative of the convolution of the image by a Gaussian. The derivative of a Gaussian (DroG) operator is

$$\nabla(g*f) = \frac{\partial(g*f)}{\partial x} + \frac{\partial(g*f)}{\partial y} = f_x + f_y \qquad (4.1.8)$$

with $g = e^{-\frac{x^2+y^2}{2\sigma^2}}$ Partial derivatives of the Gaussian function are

$$g_x(x, y) = -\frac{x}{\sigma^2} \, g,$$
$$g_y(x, y) = -\frac{y}{\sigma^2} \, g.$$

The filters are separable so we have [17]

$$g_x(x, y) = g_x(x) * g(y),$$
$$g_y(x, y) = g_y(y) * g(x).$$

50

Table 4.2: Masks for Edge Detection [18]

Kirsch	Prewitt	Sobel
$\begin{bmatrix} 5 & 5 & 5 \\ -3 & 0 & -3 \\ -3 & -3 & -3 \end{bmatrix}$	$\begin{bmatrix} 1 & 1 & 1 \\ 1 & -2 & 1 \\ -1 & -1 & -1 \end{bmatrix}$	$\begin{bmatrix} 1 & 2 & 1 \\ 0 & 0 & 0 \\ -1 & -2 & -1 \end{bmatrix}$
$\begin{bmatrix} -3 & 5 & 5 \\ -3 & 0 & 5 \\ -3 & -3 & -3 \end{bmatrix}$	$\begin{bmatrix} 1 & 1 & 1 \\ 1 & -2 & -1 \\ 1 & -1 & -1 \end{bmatrix}$	$\begin{bmatrix} 2 & 1 & 0 \\ 1 & 0 & -1 \\ 0 & -2 & -2 \end{bmatrix}$
$\begin{bmatrix} -3 & -3 & 5 \\ -3 & 0 & 5 \\ -3 & -3 & 5 \end{bmatrix}$	$\begin{bmatrix} 1 & 1 & -1 \\ 1 & -2 & -1 \\ 1 & 1 & -1 \end{bmatrix}$	$\begin{bmatrix} 1 & 0 & -1 \\ 2 & 0 & -2 \\ 1 & 0 & -1 \end{bmatrix}$
$\begin{bmatrix} -3 & -3 & -3 \\ -3 & 0 & 5 \\ -3 & 5 & 5 \end{bmatrix}$	$\begin{bmatrix} 1 & -1 & -1 \\ 1 & -2 & -1 \\ 1 & 1 & 1 \end{bmatrix}$	$\begin{bmatrix} 0 & -1 & -2 \\ 1 & 0 & -1 \\ 2 & 1 & 0 \end{bmatrix}$
$\begin{bmatrix} -3 & -3 & -3 \\ -3 & 0 & -3 \\ 5 & 5 & 5 \end{bmatrix}$	$\begin{bmatrix} -1 & -1 & -1 \\ 1 & -2 & 1 \\ 1 & 1 & 1 \end{bmatrix}$	$\begin{bmatrix} -1 & -2 & -1 \\ 0 & 0 & 0 \\ 1 & 2 & 1 \end{bmatrix}$
$\begin{bmatrix} -3 & -3 & -3 \\ 5 & 0 & -3 \\ 5 & 5 & -3 \end{bmatrix}$	$\begin{bmatrix} -1 & -1 & 1 \\ -1 & -2 & 1 \\ 1 & 1 & 1 \end{bmatrix}$	$\begin{bmatrix} -2 & -1 & 0 \\ -1 & 0 & 1 \\ 0 & 1 & 2 \end{bmatrix}$
$\begin{bmatrix} 5 & -3 & -3 \\ 5 & 0 & -3 \\ 5 & -3 & -3 \end{bmatrix}$	$\begin{bmatrix} -1 & 1 & 1 \\ -1 & -2 & 1 \\ -1 & 1 & 1 \end{bmatrix}$	$\begin{bmatrix} -1 & 0 & 1 \\ -2 & 0 & 2 \\ 1 & 0 & 1 \end{bmatrix}$
$\begin{bmatrix} 5 & 5 & -3 \\ 5 & 0 & -3 \\ -3 & -3 & -3 \end{bmatrix}$	$\begin{bmatrix} 1 & 1 & 1 \\ -1 & -2 & 1 \\ -1 & -1 & 1 \end{bmatrix}$	$\begin{bmatrix} 0 & 1 & 2 \\ -1 & 0 & 1 \\ -2 & -1 & 0 \end{bmatrix}$

Then

$$f_x = g_x(x) * g(y) * f,$$
$$f_y = g_y(y) * g(x) * f.$$

4.2   Segmentation

The word segmentation has two meanings: the procedure leading to the segmented image, and the result of such a procedure. Image segmentation is the division of an image into spatially continuous, disjointed and homogeneous regions, such that the pixels in each partitioned region possess an identical set of properties or attributes. A complete segmentation of an image R involves identification of a finite set of regions $(R_1, R_2, R_3, \ldots, R_N)$ such that

1) $R = R_1 \cup R_2 \cup R_3 \cup \ldots \cup R_N,$

2) $R_i \cap R_j = \emptyset, \quad \forall i \neq j,$

3) $P(R_i) = True, \quad \forall i,$

4) $P(R_i \cup R_j) = False, \quad i \neq j.$

Because of the variety and complexity of images, robust and efficient segmentation algorithm on digital images is still a very challenging research topic and fully automatic segmentation procedures are far from satisfying in many realistic situations. Nevertheless general approaches to segmentation can be grouped into three classes: pixel-based methods, regional methods, and edge based methods. Pixel-based methods are the easiest to understand and to implement, but are also the least powerful and, since they operate on one element at time, are particularly susceptible to noise. Continuity-based and edge-based methods approach the segmentation problem from opposing sides: edge-based methods search for differences while continuity-based methods search for similarities.

4.2.1   Pixel Based Segmentation

The most straightforward and common of the *pixel-based methods* is thresholding in which all pixels having intensity values above, or below, some level are classified as part of the segment [4]. The selection of an appropriate threshold value is usually based on a priori known properties of the object and background.

Even though image thresholding may, in many cases, seem trivial that is not usually the case. The contrast between the objects may be poor and the illumination conditions may vary and cause artefacts (such as shadows) that make the determination of appropriate threshold difficult. In addition, many applications require that the appropriate thresholds can be determined automatically [3, 11]. Image thresholding is naturally more suitable when the object intensities are smooth and almost constant inside the segments; otherwise, it fails or at least produces rough and imprecise borders with many erratically classified areas. [5]

In *bi-level thresholding*, the object and background form two different groups with distinct gray levels. All gray values greater than threshold T are assigned the object label and all other gray values are assigned the background label, thus separating the object pixels from the background pixels. In multi-level thresholding, the image is partitioned into different segments using multiple threshold values. In the first stage of the process, the image is thresholded to separate brighter regions from darker regions by locating a minimum between luminance modes of the histogram. Then histograms are formed of each of the segmented parts. If these histograms are not unimodal, the parts are thresholded again. The process continues until the histogram of a part becomes unimodal [6, 8].

4.2.2   Edge Based Segmentation

Historically, *edge-based methods* were the first set of tools developed for segmentation. To move from edges to segments, it is necessary to group edges into chains that correspond to the sides of structural units, i.e., the structural boundaries. Approaches vary in how much prior information they use, that is, how much is used of what is known about the possible shape. False edges and missed edges are two of the more obvious, and more common, problems associated with this approach. The first step in edge-based methods is to identify edges which then become candidates for boundaries.

When the boundaries are determined properly, they are formed by closed curves

and the interior of such a curve is then the sought area of a segment. In a sense, this approach also utilizes the idea of homogeneity of segmented regions; however, the requirements are much weaker: the edge is detected at locations where there is an abrupt change in the image properties, thus indicating a probable region border.

The detected region borders should be continuous and closed, reliable, and should describe the perimeters of regions with a good accuracy of localization. Unfortunately, the raw edge representation of an image as obtained by most edge detection techniques are usually far from this ideal. The obtained edges are usually disconnected, sometimes multiple or excessively thick, and many of the detected edges do not correspond to segment borders, but rather to spurious rims due to noise [5, 11].

If an image is noisy or if its region attributes differ by only a small amount between regions, a detected boundary may often be broken. *Edge linking* techniques can be employed to bridge short gaps in such a region boundary.

The edge representation is a binary image and many of the tasks (thinning, cleaning, connecting) can be done using morphological transforms. Although in some cases these operations may be based entirely on elementary morphological operations, it is often necessary to use more complicated conditional transforms that prevent undesirable side effects, such as merging edges that belong to different borders, disconnecting thin borders, etc.

Edge relaxation is another approach used to build chains from individual edge candidate pixels. This approach takes into account the local neighborhood: weak edges positioned between strong edges are probably part of the edge, while strong edges in isolation are likely spurious [4].

A variable confidence $c(t) \in (0, 1), \quad t = 1, 2, \ldots$ of being a boundary is attached to each elementary edge. These confidences are iteratively reevaluated during the relaxation procedure until all the confidences are close to either 0 or 1. Only the elementary edges with the unit final confidence will be preserved; the others will

be discarded. In each iterative step, all confidences are modified according to the current type of each elementary edge. The new confidence is calculated based on the previous one, as $c(t + 1) = \max[0, \min(1, c(t) + correction)]$ so that the result is always in the range $(0, 1)$; d may be chosen on the order of ~ 0.1. The elementary edges are classified into two classes in each iterative step: those with the confidence above a chosen threshold are considered valid, while the edges, the confidence of which dropped below the threshold, are not considered in the next step of determining the edge types [5].

4.2.3 Region Based Segmentation

Region-based methods focus our attention on an important aspect of the segmentation process we miss with point-based techniques. These techniques classify a pixel as an object pixel judging solely on its gray value independent of the context. This means that any isolated points or small areas could be classified as being object pixels, despite the fact that an important characteristic of an object is its connectivity.

Region-based image segmentation techniques differ from pixel- and edge based methods in the way they deal with spatial relationships. Region-based techniques can be all seen as region growing techniques or further divided into region growing, merging and splitting techniques, and their combinations.

There are several approaches to region growing. The algorithm may require a set of seed pixels or regions with which the process is started, or it may simply start with the initial image and process it pixel-by-pixel. If seeding is required, the seed pixels or areas may be shown interactively on screen or selected automatically. Where seeding is not required, the processing usually begins from the top left corner of the image and proceeds from left to right and top to bottom. Despite the processing details, the region growing techniques usually join neighboring pixels to a same region if their spectral properties are similar enough. The similarity can be determined in terms of a homogeneity criterion or a combination of homogeneity,

size or some other characteristics criteria.

In *region merging and splitting techniques*, the image is divided into subregions and these regions are merged or divided according to their properties. The basic idea is to start with initial regions and merge similar adjacent regions. These initial regions may be single pixels, or areas determined with help of any lowlevel segmentation technique. Region splitting methods operate in the opposite fashion; the input usually consists of large segments that are divided into smaller sub-segments with help of a simple geometric rules. If the sub-segments are not homogeneous enough, they are further divided and the process is continued [3, 8, 10].

Region Growing

Region growing refers to the procedure that groups pixels or subregions into larger regions. Starting with a set of seed points, the regions are grown from these points by including to each seed point those neighboring pixels that have similar attributes p, like intensity, gray level texture, color, etc. The following iterative procedure is then executed: For each pixel already recognized as a region member (initially for the seed), check all pixels in its neighborhood and compare the parameters p_j of these candidates with that of the seed, p_s. If the condition

$$|p_s - p_j| \leq T$$

for a particular neighboring pixel is fulfilled, add the pixel as a new member to the region; otherwise, mark it as unacceptable. The algorithm ends when there are no pixels to be added, i.e., when, for all pixels of the region, their neighbors are marked as either belonging to this region, unacceptable, or belonging to other already established regions [8].

Region Adjacency Graph The adjacency relation among the regions in a scene can be represented by a *region adjacency graph*. The regions in the scene are rep-

resented by a set of nodes $N = N_1, N_2, \ldots, N_m$, in the RAG, where node N_i, represent the region R_i, in the scene and properties of the region R_i, is stored in the node data structure N_i. The edge $e_{i,j}$ between N_i, and N_j represent the adjacency between the regions R_i, and R_j. Two regions R_i, and R_j are adjacent if there exist a pixel in region R_i, and a pixel in region R_j which are adjacent to each other.

Region Merging and Splitting

Region-merging segmentation starts with some small elementary areas that may be considered homogeneous regionspossibly and most naturally with individual pixels. Two adjacent regions may be merged when a certain criterion of homogeneity is fulfilled. The process of merging then continues until all regions are surrounded only by regions with markedly different criterion so that no further merging is possible. A simple region merging procedure as follows:

First segment the image into $R_1, R_2, \ldots, R_m$, using a set of thresholds.

For every R_i, $i = 1, 2, \ldots, m$, identify all R_j, $j \neq i$ from the RAG.

Compute an appropriate similarity measure $S_{i,j}$ between R_i and R_j, for all i and j.

If $S_{i,j} > T$, then merge R_i and R_j.

Another strategy for merging is based on the intensity of the edges between two regions. In this method, merging between adjacent regions is based on the edge intensity along the length of the demarcating boundary between two regions. If the edge intensity is small, i.e., the edge points are weak, then the two regions can be merged if the merger does not change the mean pixel intensity values considerably [6].

Splitting regions is in a sense a complementary procedure to region merging. The basic idea of region splitting is that a region that is not uniform (homogeneous) in

the sense of a chosen criterion must be split into smaller regions; this is repeated with gradually smaller regions until every region is uniform. Naturally, the already uniform regions would not be split. However, the splitting itself does not provide a satisfactory segmentation, as adjacent regions may remain split even if they fulfill the criterion for merging. Thus, the split and merge approach is usually used in segmentation. It should be mentioned that the segmentation results of both methods, region merging and split-and-merge, might differ substantially [5, 6].

Another well-known image segmentation technique is morphological *watershed transform*, which is based on mathematical morphology to divide an image due to discontinuities.

The watershed transform is a morphological algorithm usually used for the purpose of segmentation. Considering a gray level image as a topographic map, let us denote by *catchment basin* associated with a regional minimum of this map, all points whose steepest slope paths reach this minimum. The watershed line is a closed one-pixel thick crest line which separates every adjacent catchment basins, i.e., regions. In this respect this method can be classified as a region based segmentation method. We will investigate differences between classic region based methods and the watershed segmentation in Chapter 5.

4.3 Reconstruction

The goal of reconstruction is to restore a damaged or corrupted image in which part of the information has been lost. Such degradations of an image may have different origins ,such as image transmission problems and degradation in real images due to storage conditions or manipulation.

There are conventional methods like *inverse filtering, Wiener filtering* (MMSE), *Kalman filtering, algebraic approach*, etc., to restore the original object. All of these restrictions are problematic in earth remote sensing reconstruction because in all these cases we generally assume that the degrading function is known.

The problem can be described as follows: given a domain image D, a hole $M \subset D$, and an intensity u_0 known over $D - M$, we want to find an image u, an inpainting (reconstruction, restoration) of u_0, that matches u_0 outside the hole and that has acceptable content inside the hole M. This can be achieved by examining the intensity around M and *propagating* it in M. From a mathematical point of view this is an interpolation problem (See Section 3.2).

4.3.1 Propagation

We start with a seed image S_0, a mask image D, and a structuring element B. We then use dilations of S with structuring element B and masked by D in an iterative procedure as

$$S_k = [S_{k-1} \oplus B] \cap D \ \text{ until } S_k = S_{k-1}.$$

With each iteration the seed image grows (through dilation) but within the set defined by D; S propagates to fill D. Unfortunately, the computational cost of this method is extremely high. Each iteration requires $O(N^2)$ operations for an $N * N$ image and with the required number of iterations this can lead to a complexity of $O(N^3)$.

4.3.2   Morphological Reconstruction

Reconstruction is a morphological transformation involving two images and a structuring element (instead of a single image and structuring element). One image, the marker, is the starting point for the transformation. The other image, the mask, constrains the transformation. The structuring element used defines connectivity.

CHAPTER 5

METHODS

All the techniques mentioned in Chapter 4 seems to be inadequate for oceanographic data because of the inefficiency of the methods and/or structure of SST data. In this thesis, we compare these techniques and we make some changes when necessary.

5.1 Data Preparation

In this study Level 2- LAC (*Local area convergence*) SST data from MODIS-AQUA were used. Contrary to general image files, the images which we used here were big (approximately 2500×1500). Consequently, most of the CPU time is because of the data preparation stage. Choosing the data level carefully may be useful to reduce the file size and decrease the processing time. If the data include lots of properties one should eliminate unnecessary information.

HDF data are not ready for image processing before applying some processes. In this study we use MATLAB and its HDF tool to prepare the data to processing by calling necessary data with its location and some other properties. After that we find reasonable values (digital numbers) by make some conversions and combine them to reduce the efficiency of our approximations. In general *sst*, *quality_sst*, *l2_flags*, *latitude*, and *longitude* data are sufficient to get acceptably processed SST images. MATLAB code is written by me and can be found appendix.

5.2   Preprocessing

Preprocessing techniques involve those operations that are normally required prior to the main data analysis and extraction of information and are generally grouped as *radiometric* or *geometric corrections*. Radiometric corrections include correcting the data for sensor irregularities and unwanted sensor or atmospheric noise, and converting the data so they accurately represent the reflected or emitted radiation measured by the sensor. Geometric corrections include correcting for geometric distortions due to sensor-Earth geometry variations, and conversion of the data to real world coordinates (e.g., latitude and longitude) on the Earth's surface.

We applied an adaptive histogram modification algorithm for improving the visibility (written by Hakan Öktem). The algorithm is based on determining the target histogram by using the components of the original histogram over a threshold [1]. Contrary to other histogram equalization algorithms, in this technique relative distribution of the data do not change. By means of this we decide that the method is helpful to get appropriate results not only for medical images but also for ocean images by reducing lacking in contrast.

Then we used mercator image to map projection to reduce geometric degradations using latitude and longitude values. This procedure do not cause any difference in data but it restore the values to make it more understandable.

5.3   Interpolation

In this section, we concentrate on *spline interpolation* and *curve fitting* used in many image processing operations like modification, boundary tracing and reconstruction. In this thesis, we used these techniques to trace edges in segmentation procedure and to reconstruct the image. Besides, we used curve fitting to error analysis and comparison of methods' accuracy with respect to root mean square error.

5.3.1 Spline Interpolation

Splines are interpolative polynomials that involve information concerning the derivative of the function at certain points. Unlike Hermite interpolation that explicitly invokes knowledge of the derivative, splines utilize that information implicitly so that specific knowledge of the derivative in not required. Unlike general interpolation formulae of the Lagrangian type, which maybe used in a small section of a table, splines are constructed to fit an entire run of tabular entries of the independent variable. While one can construct splines of any order, the most common ones are cubic splines as they generate tri-diagonal equations for the coefficients of the polynomials [8, 21].

Spline (spliced line) interpolation is a particular kind of *piecewise polynomial interpolation*. We may wish, for example, to approximate $f(x)$ for $x \in [a, b] \subset \mathbb{R}$ when given the sample points $\{(x_k, f(x_k)) | k \in \mathbb{Z}_{n+1}\}$ by fitting straight-line segments in between $(x_k, f(x_k))$, and $(x_{k+1}, f(x_{k+1}))$ for $k = 0, 1, \ldots, n-1$. An example of this appears in Figure 5.1.

This has a number of disadvantages. Although $f(x)$ may be differentiable at $x = x_k$, the piecewise linear approximation will not be (in general). Also, the graph of the interpolant has visually displeasing kinks in it. If interpolation is for a computer graphics application, or to define the physical surface of an automobile body or airplane, then such kinks are seldom acceptable. Splines are a means to deal with this problem.

Definition (Spline)[22] :

Suppose that we are given $\{(x_k, f(x_k)) | k \in \mathbb{Z}_{n+1}\}$. The piecewise polynomial function $p_m(x)$ is called a *spline* if

$(S1)$ $p_m(x_k) = f(x_k)$ for all $k \in \mathbb{Z}_{n+1}$ (interpolation).

$(S2)$ $\lim_{x \to x_k^-} p_m^{(i)}(x) = \lim_{x \to x_k^+} p_m^{(i)}(x)$ for all $i \in \mathbb{Z}_{N+1}$ (smoothness).

$(S3)$ $p_m(x)$ is a polynomial of degree no larger than m on every subinterval $[x_k, x_{k+1}]$ for $k \in \mathbb{Z}_n$ (interval of definition).
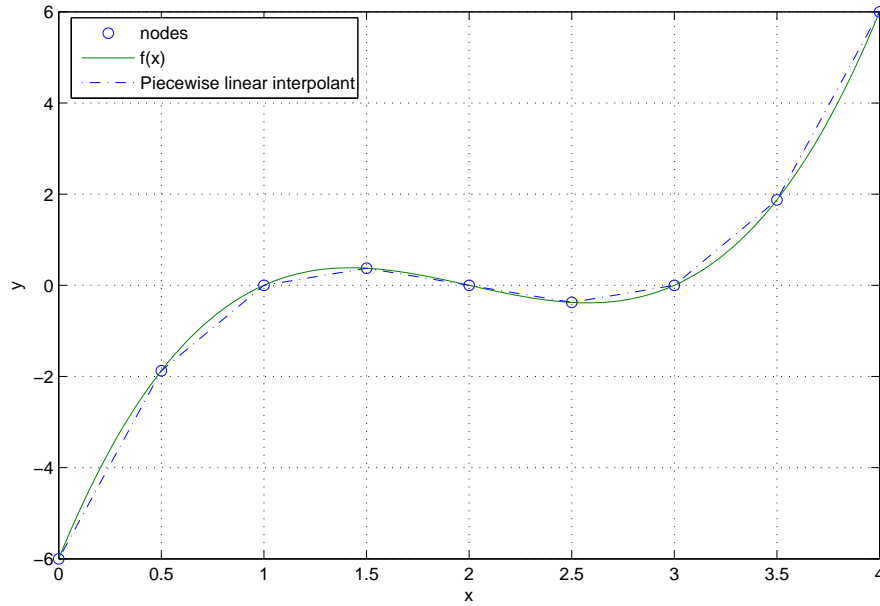
Figure 5.1: The cubic polynomial $f(x) = (x-1)(x-2)(x-3)$, and its piecewise linear interpolant (dashed line) at the nodes $x_k = x_0 + hk$ for which $x_0 = 0$, and $h = \frac{1}{2}$, where $k = 0, 1, \ldots, n$ with $n = 8$.

We say that m is the *degree of approximation* and N is the *degree of smoothness* of the spline $p_m(x)$.

There is a relationship between m and N. As there are n subintervals $[x_k, x_{k+1}]$, and each of these is the domain of definition of a degree m polynomial, we see that there are $D_f = n(m+1)$ *degrees of freedom*. Each polynomial is specified by $m+1$ coefficients, and there are n of these polynomials; hence D_f is the number of parameters to solve for in total. From the definition there are

$n+1$ interpolation conditions (axiom (S1)). And there are $n-1$ junction points $x_1, \ldots, x_{n-1}$ (sometimes also called *knots*), with $N+1$ continuity conditions being imposed on each of them (axiom (S2)). As a result, there are $D_c = (n+1) + (n-1)(N+1)$ *constraints*. Consider

$$D_f - D_c = n(m+1) - [(n+1) + (n-1)(N+1)] = n(m-N-1) + N. \quad (5.3.1)$$

65

It is a common practice to enforce the condition $m - N - 1 = 0$; that is, we let

$$m = N + 1. \tag{5.3.2}$$

This relates the degree of approximation to the degree of smoothness in a simple manner [10, 11, 37].

Example

Figure 5.2 shows the natural and complete cubic spline interpolants to the function $f(x) = e^{-x^2}$ for $x \in [-1, 1]$. We have chosen the nodes $x_k = -1 + \frac{1}{2}k$, for $k = 0, 1, 2, 3, 4$ (i.e., $n = 4$, and $h = \frac{1}{2}$). Clearly, $f'(x) = -2xe^{-x^2}$. Thus, at the nodes

$$f(\pm 1) = 0.36787944, \qquad f(\pm\frac{1}{2}) = 0.60653066, \qquad f(0) = 1.00000000,$$

and

$$f'(\pm 1) = \mp 0.73575888.$$
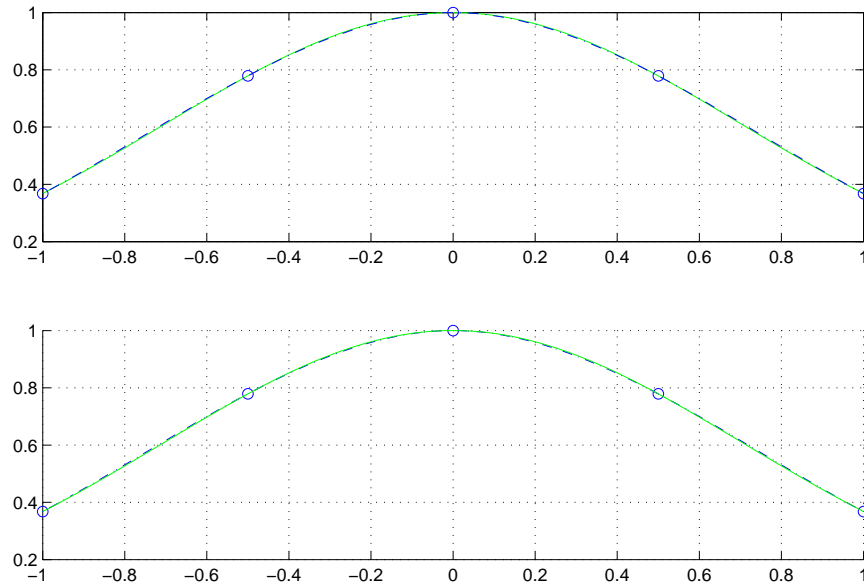
Figure 5.2: Natural and complete (respectively) spline interpolants (dashed lines) for the function $f(x) = e^{-x^2}$ (solid lines) on the interval $[-1, 1]$. The circles correspond to node locations. Here $n = 4$, with $h = 12$, and $x_0 = -1$. The nodes are at $x_k = x_0 + h_k$ for $k = 0, \ldots, n$.

Of course, the spline series for our example has the form

$$p_3(x) = \sum_{k=-1}^{5} a_k S_k(x),$$

so we need to determine the coefficients a_k. Considering the natural spline interpolant first, we have

$$\begin{bmatrix} 4 & 1 & 0 \\ 1 & 4 & 1 \\ 0 & 1 & 4 \end{bmatrix} \begin{bmatrix} a_1 \\ a_2 \\ a_3 \end{bmatrix} = \begin{bmatrix} f(x_1) - \frac{1}{6}f(x_0) \\ f(x_2) \\ f(x_3) - \frac{1}{6}f(x_4) \end{bmatrix}.$$

Additionally,

$$a_0 = \frac{1}{6}f(x_0) = \frac{1}{6}f(-1), \qquad a_4 = \frac{1}{6}f(x_4) = \frac{1}{6}f(1),$$

and

$$a_{-1} = f(x_0) - 4a_0 - a_1, \qquad a_5 = f(x_4) - 4a_4 - a_3.$$

The natural spline series coefficients are therefore

k	a_k
-1	-0.01094139
0	0.06131324
1	0.13356787
2	0.18321607
3	0.13356787
4	0.06131324
5	-0.01094139

Now, on considering the case of the complete spline, we have

$$
\begin{bmatrix}
4 & 2 & 0 & 0 & 0 \\
1 & 4 & 1 & 0 & 0 \\
0 & 1 & 4 & 1 & 0 \\
0 & 0 & 1 & 4 & 1 \\
0 & 0 & 0 & 2 & 4
\end{bmatrix}
\begin{bmatrix}
a_0 \\
a_1 \\
a_2 \\
a_3 \\
a_4
\end{bmatrix}
=
\begin{bmatrix}
f(x_0) + \frac{1}{3}hf'(x_0) \\
f(x_1) \\
f(x_2) \\
f(x_3) \\
f(x_4) - \frac{1}{3}hf'(x_4)
\end{bmatrix}.
$$

Additionally

$$
a_{-1} = a_1 - \frac{1}{3}hf'(x_0), \qquad a_5 = a_3 + \frac{1}{3}hf'(x_4).
$$

The complete spline series coefficients are therefore

k	a_k
-1	0.01276495
0	0.05493076
1	0.13539143
2	0.18230428
3	0.13539143
4	0.05493076
5	0.01276495

This example demonstrates that the complete spline interpolant tends to be more accurate than the natural spline interpolant. However, accuracy of the complete spline interpolant is contingent on accurate estimation, or knowledge of the derivatives $f'(x_0)$ and $f'(x_n)$ [37].

5.3.2   Minimum Mean-Square Error Curve Fitting

Finding a function (curve) $y = f(x)$ that best fits a set of measured x values and corresponding y values is called *curve fitting process*. The commonly-used measure of fit in curve fitting is mean-squared error (MSE). In minimum mean-squared error (MMSE) curve fitting (also called *least-square curve fitting*), the

parameters of a selected function are chosen to minimize the MSE between the curve and the measured values.

Polynomial regression is a form of MMSE curve fitting in which the selected function is a polynomial and the parameters to be chosen are the polynomial coefficients.

Linear regression is a form of polynomial regression in which the polynomial is of first degree. The two parameters of a linear equation, representing a straight line curve, are chosen to minimize the average of the squared distances between the line and the measured data values [10,22].

Linear Regression

To illustrate linear regression, consider the following set of temperature measurements:

Time (s)	Temperature (F)
0	0
1	20
2	60
3	68
4	77
5	110

Observing the plot of these data points shown in Figure 5.3, it can be seen that a good estimate of a line passing through the points is $y = 20x$.

A measure of the quality of the fit of the linear estimate to the data is the *mean squared error (MSE)* or the *root mean squared error (RMSE)*

$$MSE = \frac{1}{N} \sum_{k=1}^{N} (\hat{y}_k - y_k)^2,$$
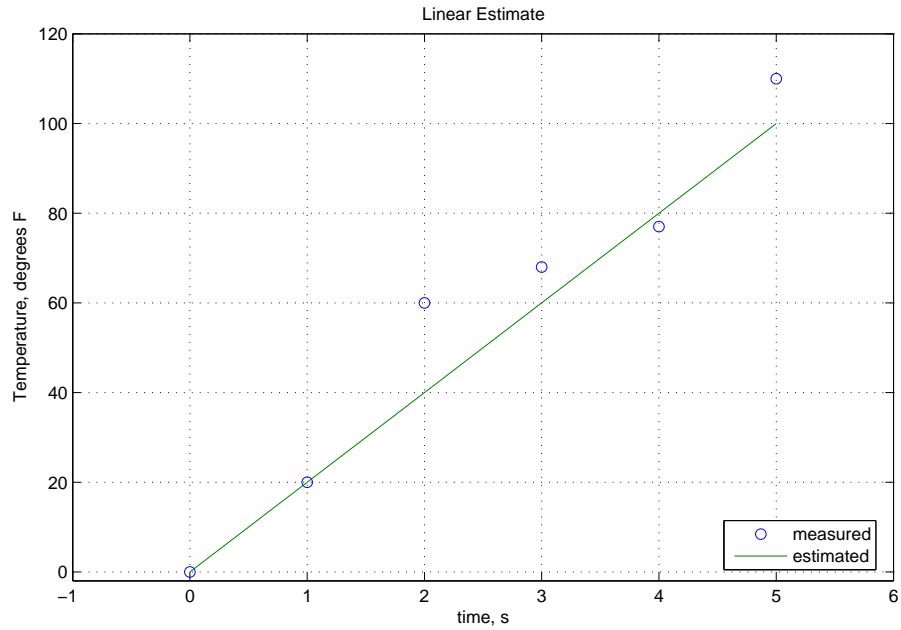
$$RMSE = \sqrt{MSE}, \tag{5.3.3}$$

Figure 5.3: A linear estimate

where N is the number of measured data values (x_k, y_k), with estimated values $\hat{y}_k = 20x_k$. For this estimation we find that $MSE = mean((\hat{y} - y)^2) = 95.5000$ and $RMSE = \sqrt{MSE} = 9.7724$ Note that the absolute values of the errors in the estimates range from zero to 20, so an RMSE value of about 10 seems reasonable.

The best fit is the line $\hat{y} = a_1 x + a_2$ having coefficients a_1 and a_2 that produce the smallest mean squared error (MSE). MSE is expressed as

$$
\begin{aligned}
MSE &= \frac{1}{N} \sum_{k=1}^{N} (\hat{y}_k - y_k)^2, \\
&= \frac{1}{N} \sum_{k=1}^{N} (a_1 x_k + a_2 - y_k)^2.
\end{aligned}
\tag{5.3.4}
$$

The MSE is minimum when its partial derivatives with respect to each of the coefficients are zero:

$$\frac{\partial MSE}{\partial a_1} = \frac{1}{N} \sum_{k=1}^{N} 2(a_1 x_k + a_2 - y_k) x_k$$

$$= \frac{2}{N} \sum_{k=1}^{N} a_1 x_k^2 + a_2 x_k - x_k y_k$$

$$= \frac{2}{N} \left[\left(\sum_{k=1}^{N} x_k^2 \right) a_1 + \left(\sum_{k=1}^{N} x_k \right) a_2 - \left(\sum_{k=1}^{N} x_k y_k \right) \right]$$

$$= 0.$$

$$\frac{\partial MSE}{\partial a_2} = \frac{1}{N} \sum_{k=1}^{N} 2(a_1 x_k + a_2 - y_k)$$

$$= \frac{2}{N} \left[\left(\sum_{k=1}^{N} x_k \right) a_1 + N a_2 - \left(\sum_{k=1}^{N} y_k \right) \right]$$

$$= 0.$$

Ignoring the constant factors $\frac{2}{N}$ and writing the two equations above in matrix form with the terms in the unknown coefficients a_1 and a_2 on the left hand side

$$\begin{bmatrix} \sum_{k=1}^{N} x_k^2 & \sum_{k=1}^{N} x_k \\ \sum_{k=1}^{N} x_k & N \end{bmatrix} \begin{bmatrix} a_1 \\ a_2 \end{bmatrix} = \begin{bmatrix} \sum_{k=1}^{N} x_k y_k \\ \sum_{k=1}^{N} y_k \end{bmatrix}.$$

Solving this system of linear equation in two unknowns we find the best linear fit as $\hat{y} = 20.8286x + 3.7619$ and the root mean squared error is 7.71, lower than that of the previous estimate.

Polynomial Regression The method discussed above for linear regression can be extended to an n-th degree polynomial curve fit, using a method known as *polynomial regression* to find the minimum mean squared error values of the polynomial coefficients. The n-th degree polynomial in one variable is

$$f(x) = a_1 x^n + a_2 x^{n-1} + a_3 x^{n-2} + \ldots + a_n x + a_n + 1$$

This provides an n-th degree least-squares polynomial curve fit to the vectors x

and y, which must be of the same length. It returns a coefficient vector a of length $n+1$. As the degree increases, the MSE decreases and the number of points that fall on the curve increases. If a set of $n+1$ points is used to determine the n-th degree polynomial, all $n+1$ points will fall on the polynomial curve. Regression analysis cannot determine a unique solution if the number of points is equal to or less than the degree of the polynomial model [10, 14, 15].

Theorem 2.2 *Least Squares Parabola* :

Suppose that $\{(x_k, y_k)\}_{k=1}^{N}$ are N points where the abscissas are distinct. The coefficients of the least square parabola

$$y = f(x) = Ax^2 + Bx + C \tag{5.3.5}$$

are the solution values A, B and C of the linear system

$$\left(\sum_{k=1}^{N} x_k^4\right) A + \left(\sum_{k=1}^{N} x_k^3\right) B + \left(\sum_{k=1}^{N} x_k^2\right) C = \sum_{k=1}^{N} y_k x_k^2$$

$$\left(\sum_{k=1}^{N} x_k^3\right) A + \left(\sum_{k=1}^{N} x_k^2\right) B + \left(\sum_{k=1}^{N} x_k\right) C = \sum_{k=1}^{N} y_k x_k \tag{5.3.6}$$

$$\left(\sum_{k=1}^{N} x_k^2\right) A + \left(\sum_{k=1}^{N} x_k\right) B + NC = \sum_{k=1}^{N} y_k$$

Proof :

The coefficients A, B and C will minimize the quantity

$$e(A, B, C) = \sum_{k=1}^{N} (Ax_k^2 + Bx_k + C - y_k)^2. \tag{5.3.7}$$

The partial derivatives $\frac{\partial e}{\partial A}$, $\frac{\partial e}{\partial B}$, and $\frac{\partial e}{\partial C}$ must all be zero. This results in

$$0 = \frac{\partial e(A, B, C)}{\partial A} = 2 \sum_{k=1}^{N} (Ax_k^2 + Bx_k + C - y_k)^1 (x_k^2)$$

$$0 = \frac{\partial e(A, B, C)}{\partial B} = 2 \sum_{k=1}^{N} (Ax_k^2 + Bx_k + C - y_k)^1 (x_k) \qquad (5.3.8)$$

$$0 = \frac{\partial e(A, B, C)}{\partial C} = 2 \sum_{k=1}^{N} (Ax_k^2 + Bx_k + C - y_k)^1 (1)$$

Using the distributive property of addition, we can move the values A,B, and C outside the summations in (5.3.8) to obtain the normal equations that are given in (5.3.6).

Example Find the least squares parabola for the four points $(-3, 3)$, $(0, 1)$, $(2, 1)$, and $(4, 3)$.

The linear system (5.3.6) for finding A, B, and C becomes

$$353A + 45B + 29C = 79$$
$$45A + 29B + 3C = 5$$
$$29A + 3B + 4C = 8.$$

The solution to the linear system is $A = 585/3278$, $B = -631/3278$, and $C = 1394/1639$ and the desired parabola is (see Figure 5.4).

$$y = \frac{585}{3278}x^2 - \frac{631}{3278}x + \frac{1394}{1639} = 0.178462x^2 - 0.192495x + 0.850519.$$

5.4   Edge Detection

Over the last decade, various edge detection methods have been applied into oceanographic satellite images. Although the significant improvements have been made in edge detection methods, there may be problems when using the algorithms for satellite derived SST images. Due to the degradation and corruption
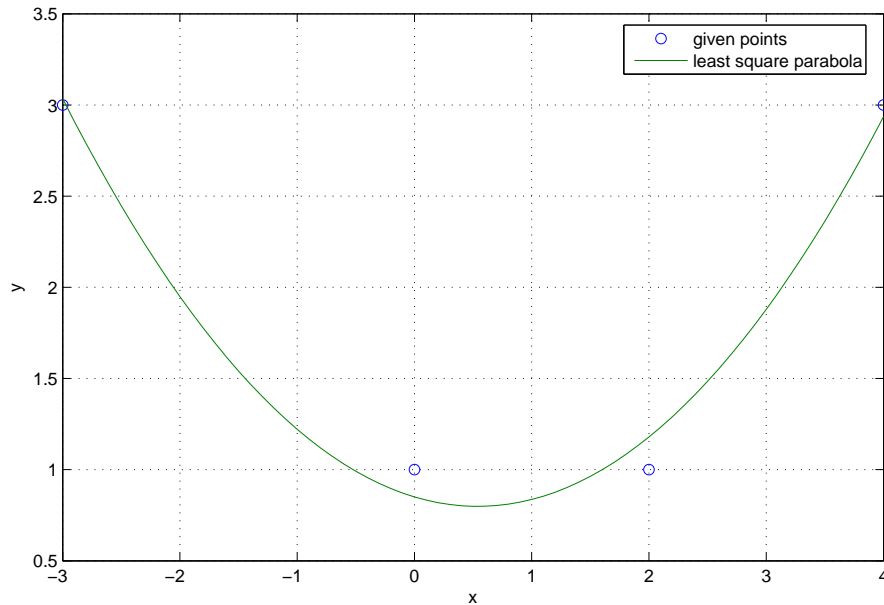
Figure 5.4: The least squares parabola for the points $(-3, 3)$, $(0, 1)$, $(2, 1)$, and $(4, 3)$.

of oceanographic images, discontinuities and false edges may occur. In this stage we applied Canny method after histogram modification algorithm.

5.4.1 Canny Edge Detector

Canny detector (Canny [1986]) is one of the most powerful edge detectors. The method has three simultaneous goals: low rate of detection errors, good edge localization, and only a single detection response per edge. Canny assumed that false-positive and false-negative detection errors are equally undesirable and so gave them equal weight.

The edge detection filters, mentioned previously, have some interesting properties. Each mask includes a derivative of Gaussian function to perform the nearly optimal directional derivative across the intended edge. A smooth, averaging profile appears in the mask along the intended edge direction in order to reduce

noise without compromising the sharpness of the edge profile. In the smoothing direction, the filter extent is usually several times that in the derivative direction when the filter is intended for straight edges. Canny's method includes a *goodness of fit* test to determine if the selected filter is appropriate before it is applied. The test examines the gray-level variance of the strip of pixels along the smoothing direction of the filter. If the variance is small, then the edge must be close to linear, and the filter is a good choice. A large variance indicates the presence of curvature or a comer, in which case a better choice of filter would have smaller extent in the smoothing direction [18, 20].

The method can be summarized as follows:

The image is smoothed using a Gaussian filter with a specified standard deviation, σ, to reduce noise.

The local gradient, and edge direction are computed at each point. An edge point is defined to be a point whose strength is locally maximum in the direction of the gradient.

The edge points determined in the previous step give rise to ridges in the gradient magnitude image. The algorithm then tracks along the top of these ridges and sets to zero all pixels that are not actually on the ridge top so as to give a thin line in the output, a process known as *nonmaximal suppression*. The ridge pixels are then thresholded using two thresholds, Tl and $T2$, with $Tl < T2$. Ridge pixels with values greater than $T2$ are said to be *strong* edge pixels. Ridge pixels with values between $T1$ and $T2$ are said to be *weak* edge pixels.

Finally, the algorithm performs edge linking by incorporating the weak pixels that are 8-connected to the strong pixels.

Figure 5.6, 5.7, and 5.8 shows edges of Figure 5.5 detected by using *Sobel*, *Canny* and edge traced Canny, respectively. One can easily understand that Sobel is not selective about strongness of edges so Figure (5.6) includes individual edges everywhere. Canny method differs weak and strong edges but it requires very small threshold (here 0.03). Such a low threshold (Figure 5.6 threshold is 0.3)
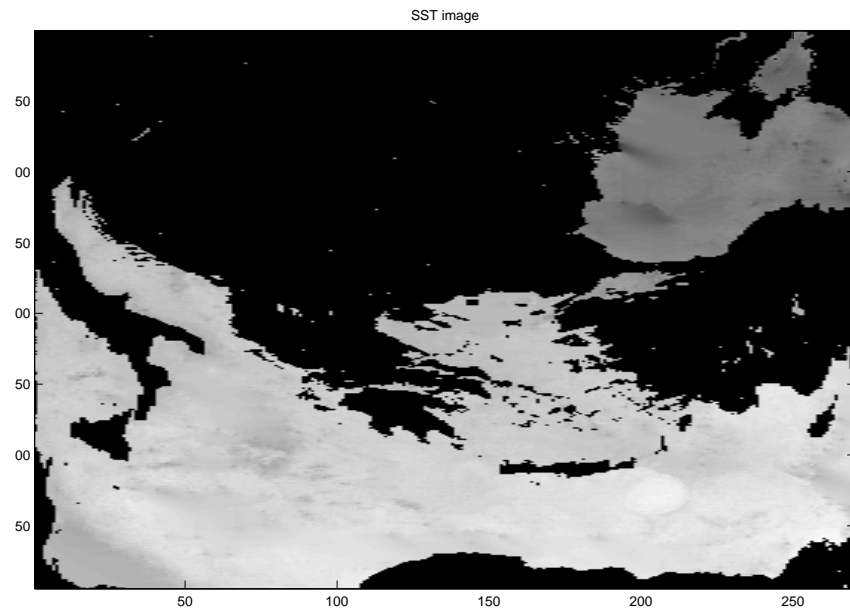
Figure 5.5: SST image

can cause wrong decisions. We can use an edge tracing method to link distinct edges and we set to 'not edge' if a point does not have any strong edge in its 4 or 8 neighborhood (See Figure 5.8).
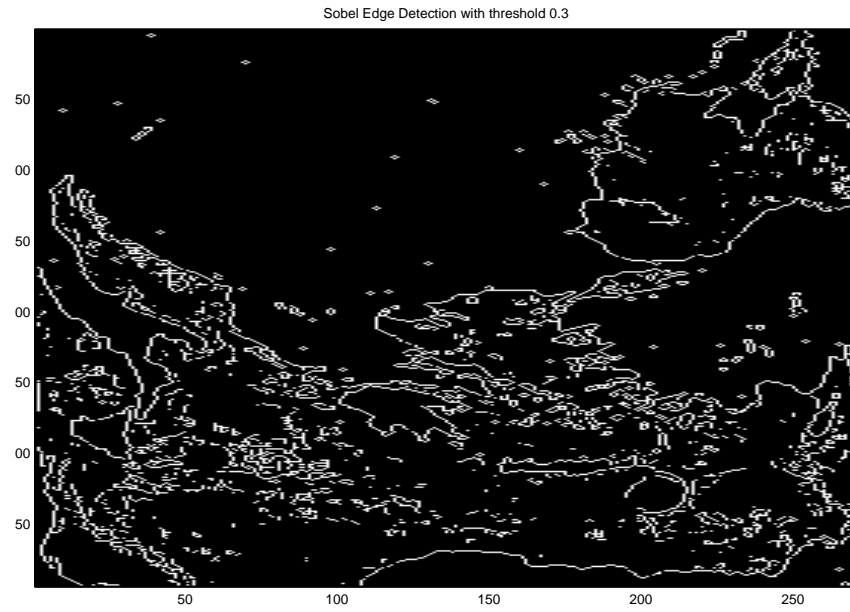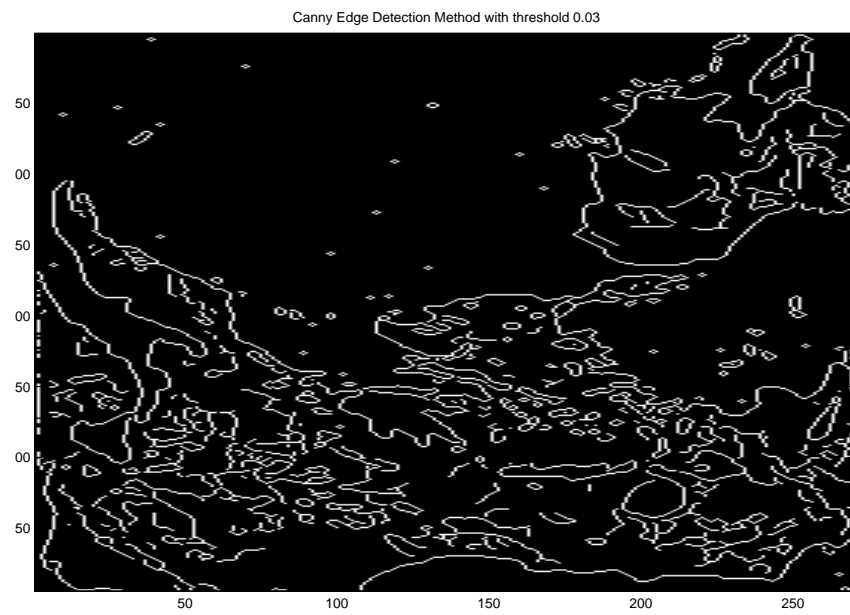
Figure 5.6: Sobel method
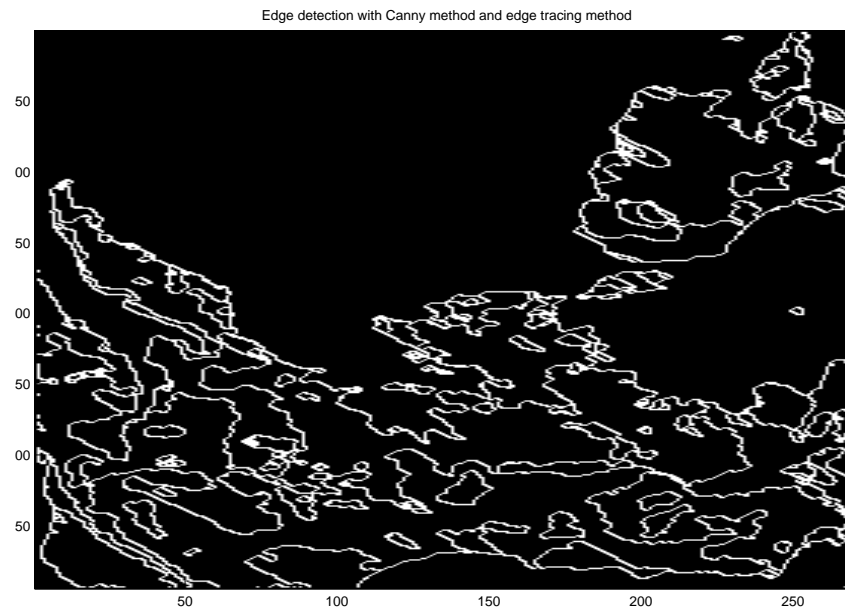

Figure 5.7: Canny method

78

Figure 5.8: Combination of Canny and Edge Tracing Method

5.5 Segmentation

While humans may look at a displayed image and recognize its structure readily, the computer must algorithmically analyze the array of image pixel values before it can reach any conclusions about the content of the image. Computer analysis of images usually starts with a process called segmentation.

5.5.1 Watershed Segmentation

The watershed transform is a morphological algorithm usually used for the purpose of segmentation. Considering a gray level image as a topographic map,let us denote by *catchment basin* associated with a regional minimum of this map, all points whose steepest slope paths reach this minimum. The watershed line is a closed one-pixel thick crest line which separates every adjacent catchment basins, i.e., regions.

The strength of watershed segmentation is that it produces a unique solution for a particular image, and it can be easily adapted to any kind of digital grid and extended to $n-$dimensional images and graphs. However, direct application of the watershed transform to a gradient image usually leads to oversegmentation due to noise and other local irregularities of the gradient. The resulting problems can be serious enough to render the result virtually useless. Another disadvantage of watershed segmentation related to the image noise and the images discrete nature, is that the final boundaries of the segmented region are lack of smoothness.

These disadvantages could be reduce by *Marker controlled watershed segmentation.* This approach is applied as follows: first, we define the properties which will be used to mark the objects, i.e., the homogeneous regions can be marked by minima of the gradient. These markers are called object markers. The same is done for the background, i.e., for portions of the image in which we are sure there is no pixel belonging to any object. These markers constitute the background markers. The rest of the procedure is straightforward and is the same for all applications : the gradient image is modified in order to keep only the most significant contours in the areas of interest between the markers. Then we perform the final contour search on the modified gradient image by using the watershed transformation. Generally the gradient image is used in the watershed transformation, because the main criterion of the segmentation is the homogeneity of the grey values of the objects present in the image [3, 49].

5.5.2   Results

Ocean structures are difficult to segment properly because gradients are weak and provide excess of information and due to the presence of noise, mainly due to clouds and other atmospheric phenomena. We choose an unsharp masking contrast enhancement filter h to improve the visual quality to enhance the edges (gradients) of our image:

$$h = \frac{1}{\alpha + 1} \begin{bmatrix} -\alpha & \alpha - 1 & -\alpha \\ \alpha - 1 & \alpha + 5 & \alpha - 1 \\ -\alpha & \alpha - 1 & -\alpha \end{bmatrix}. \qquad (5.5.9)$$

Due to discontinuities of edge lines, the image do not include concrete objects and, hence, another operation is necessary for linking these edges. We use an edge tracing algorithm which depends on the edge direction, and the image is partitioned into disjointed regions (i.e., segmented) according to these boundaries. The process searches neighbor pixels until it access the same start point (pixel) in determined region. If there is no possibility of continuity in any direction the method fails. Fortunately this situation occurs only if the edges of the objects have intersection.

Figure (5.9) and (5.10) simply show that watershed segmentation is not adequate for ocean images even if we control oversegmentation/undersegmentation probability.

5.6 Reconstruction

All of remote sensing sources contain uncertainties which cannot be completely quantified. Even the most reliable of all available climate data, the instrumental records, may contain random, systematic or time-varying biases (Jones et al. 1999). Due to mechanical problems, out-of-focus blur, motion, inappropriate illumination, and noise the quality of the digitized image can be inferior to the original. *Image enhancement*: In order to aid visual interpretation, the visual appearance of the objects in the image can be improved by techniques such as grey level stretching to improve the contrast and spatial filtering for enhancing the edges. *Image restoration* or rectification techniques, are intended to correct for sensor- and platform-specific radiometric and geometric distortions of data. Radiometric corrections may be necessary due to variations in scene illumination and viewing geometry, atmospheric conditions, and sensor noise and response. In
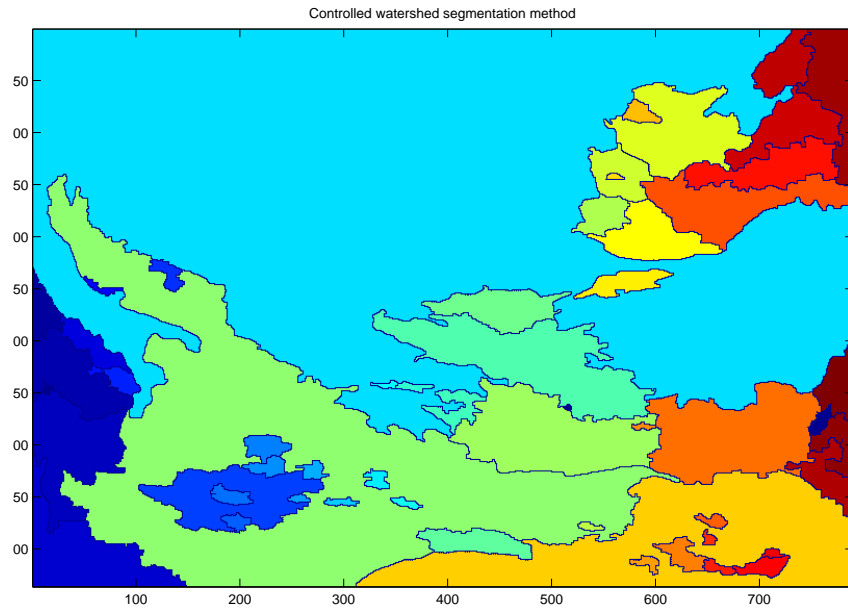
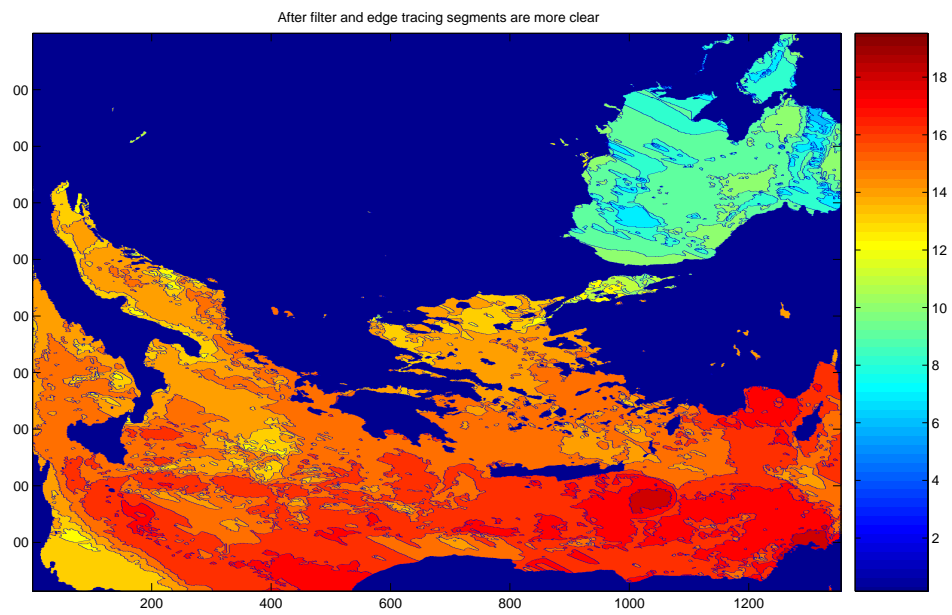Figure 5.9: Controlled Watershed Segmentation Method

Figure 5.10: Filtered and Traced image

order to actually geometrically correct the original distorted image, a procedure called *resampling* is used to determine the digital values to place in the new pixel locations of the corrected output image. All these techniques aim that make understandable and clear already available data for last user. However oceanographic images are not completely visible and cloud is the most important reason of this shortage.

In this thesis, we use only the satellite data with the quality level 0, this quality level assigned to the data pixels free from any problems that may occur in satellite data processing due to large solar zenith angles, clouds, sun glint contamination, shallow water, negative radiance retrievals, failed atmospheric correction. We approximate an unknown pixel by using the nearest four known pixels' temperature values without consideration of other parameters such as salinity, height, etc. These values have inverse rate effect with respect to their distances from unknown pixel (See Appendix):

$$sst(i,j) = \frac{e}{\alpha}\left(\frac{s_e}{e} + \frac{s_n}{n} + \frac{s_w}{w} + \frac{s_s}{s}\right), \tag{5.6.10}$$

where $sst(i,j)$ is unknown pixel, s is the distance from nearest south pixel, s_s is the temperature of this pixel, e is the distance from nearest east pixel, s_e is the temperature of this pixel, n is the distance from nearest north pixel, s_n is the temperature of this pixel, w is the distance from nearest west pixel, s_w is the temperature of this pixel and $\alpha = 1 + \frac{e}{n} + \frac{e}{w} + \frac{e}{s}$.

Figures 5.12, 5.13 and 5.14 are results of reconstruction of image (see Figure 5.11) by polynomial fitting, by cubic spline interpolation and by distance based method explained above. We choose two regions from image and set these regions to unknown pixels to test our method. One of the regions is chosen less homogeneous since we can easily realize the methods efficiency.

Number of unknown pixels in the image = 55000.

Number of the finding pixels after reconstruction
polynomial fitting = 48511 in 1m30 seconds,

cubic spline interpolation =52123 in 21 seconds,

our technique = 52123 in 2m 17seconds,

rmse (1)= 2,2684,

rmse (2) = 5,78,

rmse (3) = 0.31,

According to rmse (root mean square error) one can think that polynomial fitting gives more reasonable result than cubic spline interpolation but polynomial fitting is much more sensitive if some pixels are really different than other pixels and so this may be cause of unacceptable deviation in reconstructed pixel. In this example one of the missing pixels is evaluated as 31 while actual value is 26 which is a fatal error in SST images. Thus we can only prefer polynomial fitting if data is almost complete but this situation is also so rare in oceanography. From these results we can say that our technique is more efficient than interpolation techniques but its CPU time is more than others. According to percentage of unknown pixels (up to 35) our method can be chosen for reconstruction of oceanographic data.
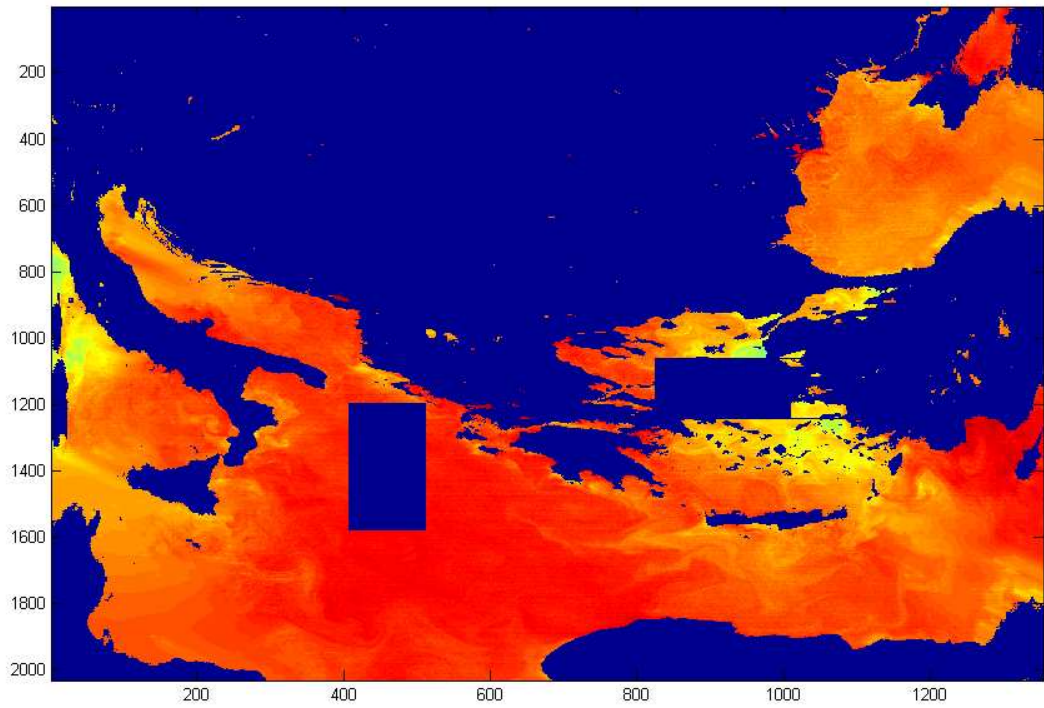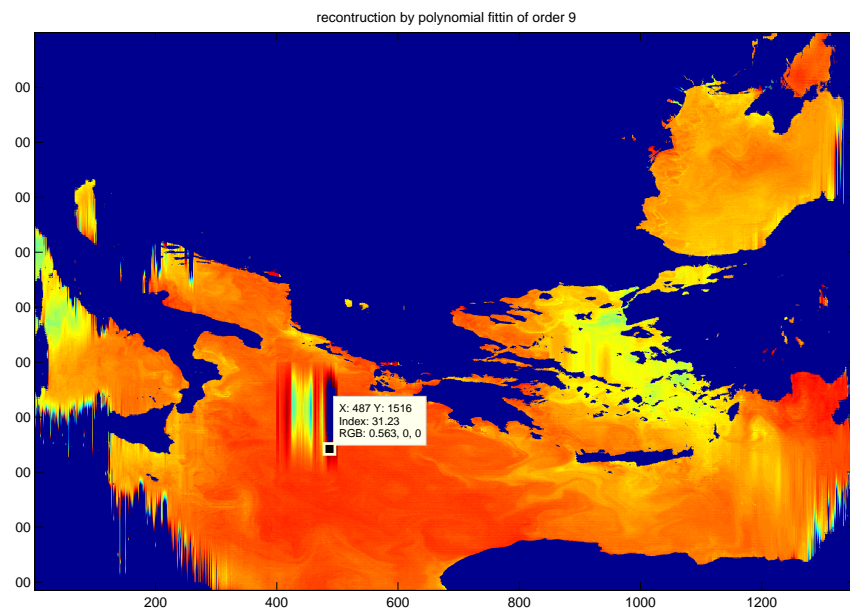
Figure 5.11: Incomplete image
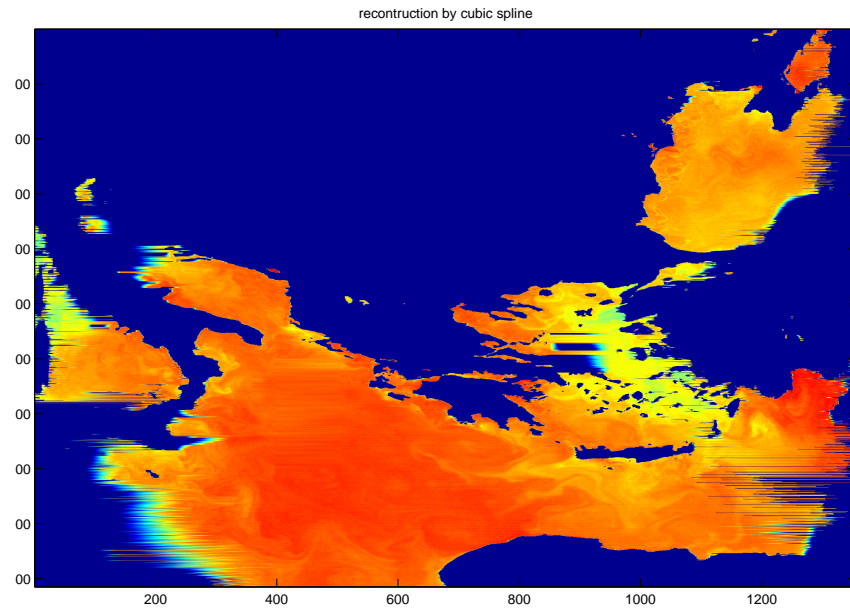

Figure 5.12: Fitting image

Figure 5.13: Interpolation of missing data

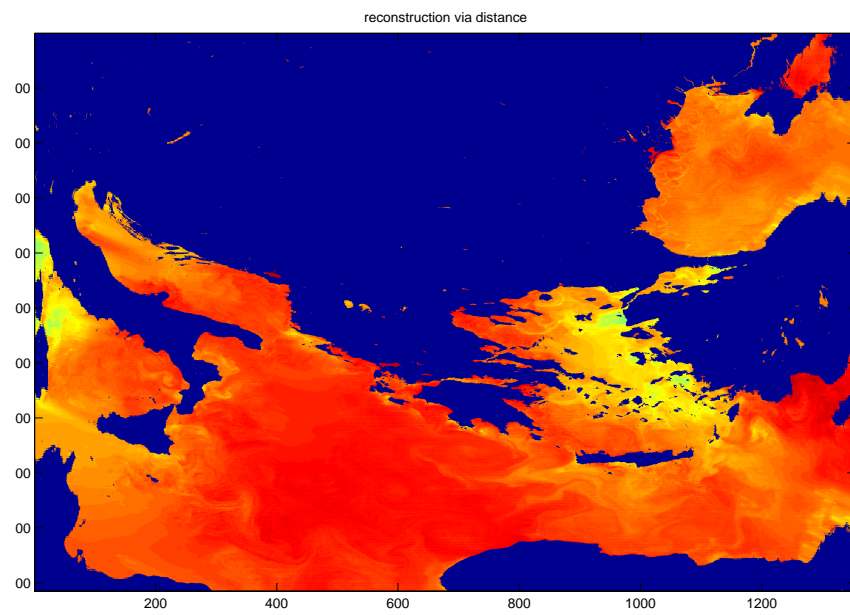Figure 5.14: Better reconstruction

CONCLUSIONS AND FUTURE WORK

6.1 Conclusions

Image processing techniques which have convenient results when applied to an image (e.g., medical, forestry, or photographic) may have inconvenient results when we apply these techniques to an oceanographic image. This is because images have different characteristics with respect to belonging area and/or sensor.

Since our data are from MODIS which is more sensitive comparison to other satellites, and some atmospheric- systematic corrections are done before we get the data, in addition by the help of quality data we choose quality level 0 to reduce noise in this data we need not much preprocessing techniques. Thus, in this study we did not give much place to preprocessing techniques. We can not get constructive results from other histogram techniques then we applied an adaptive histogram modification algorithm over our image. (See Figure 6.2)
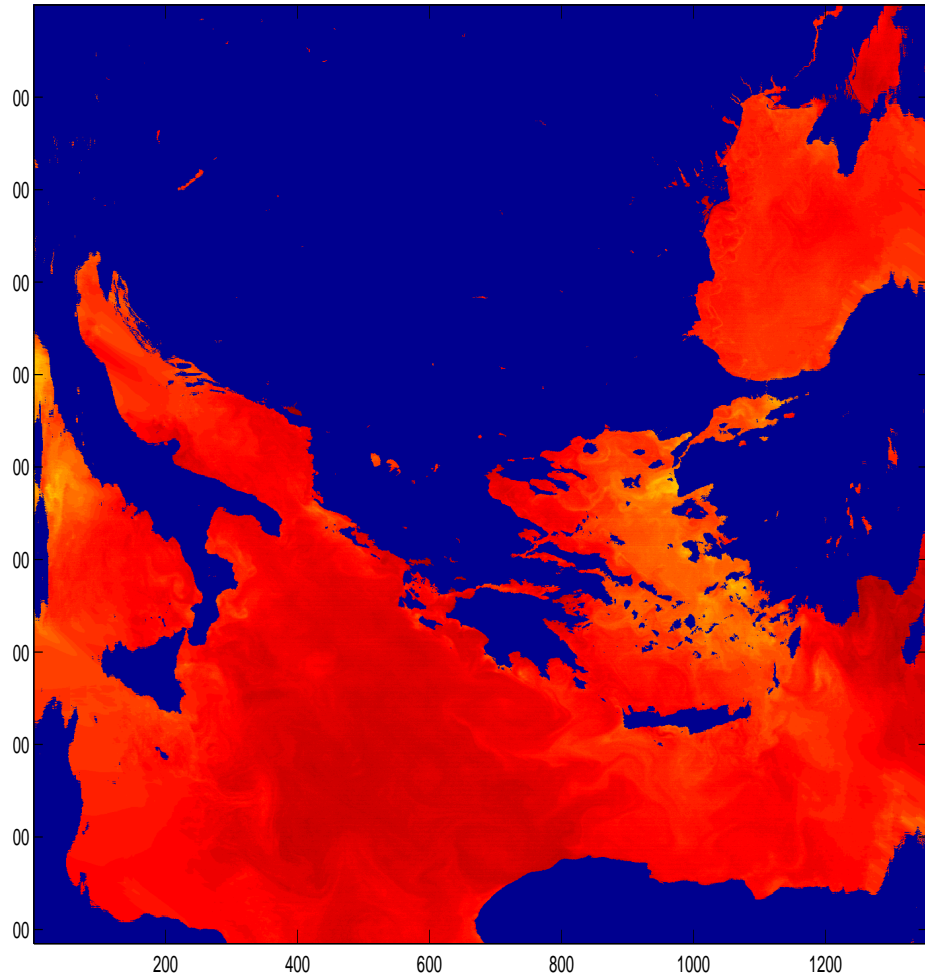
Figure 6.1: Before Adaptive Histogram Modification algorithm.

There are many image segmentation methods in literature generally based on edge detection, growth of homogeneous regions conditional upon similarities between pixels or mathematical morphology. Edge based and region based algorithms performance is insufficient because of deficiencies of SST images. In contrast to classical segmentation algorithms, the watershed transform has several advantages including the proper handling of gaps and the placement of boundaries at the most significant edges. But watershed segmentation algorithm requires gradient image and we need another control statement to reduce oversegmentation. Due to incompleteness of ocean image which we want to segment have approximate values (even if we reconstruct) so that performance of algorithm decrease.

Most of all, the incompleteness of our data make all the process more difficult. Thus our main purpose is reconstructing the data. Most of reconstruction (or estimation) techniques such as interpolation, curve fitting, polynomial fitting give accurate results when we are dealing with an image less than 10-15 percent missing pixels. Polynomial fits are unstable in the sense that the values the polynomials give at points between the stations vary greatly for small changes in the data at the station points, and especially so when data are missing. The problem gets worse as the order of the polynomial is increased. The method is nearly useless where the data are sparse. The instability of the polynomial fit is such that when one key data point is removed, the polynomial fit in that region may change radically.

Our method find the unknown pixels using known pixels and distances (see Appendix) but it gives accurate results only if image is not dense. Also CPU time is not so short and there may be wrong estimates if the values change rapidly. To understand the efficiency of this algorithm and make comparison look figure and tables.

We can easily understand that raw data (Figure 6.1) have unqualified data, i.e. same of the pixels are less than -2 which is an unacceptable situation for oceanographic images. Figure 6.2 we see much gaps since inaccurate pixels (cloud and nhd) eliminated by using converthdf.m.
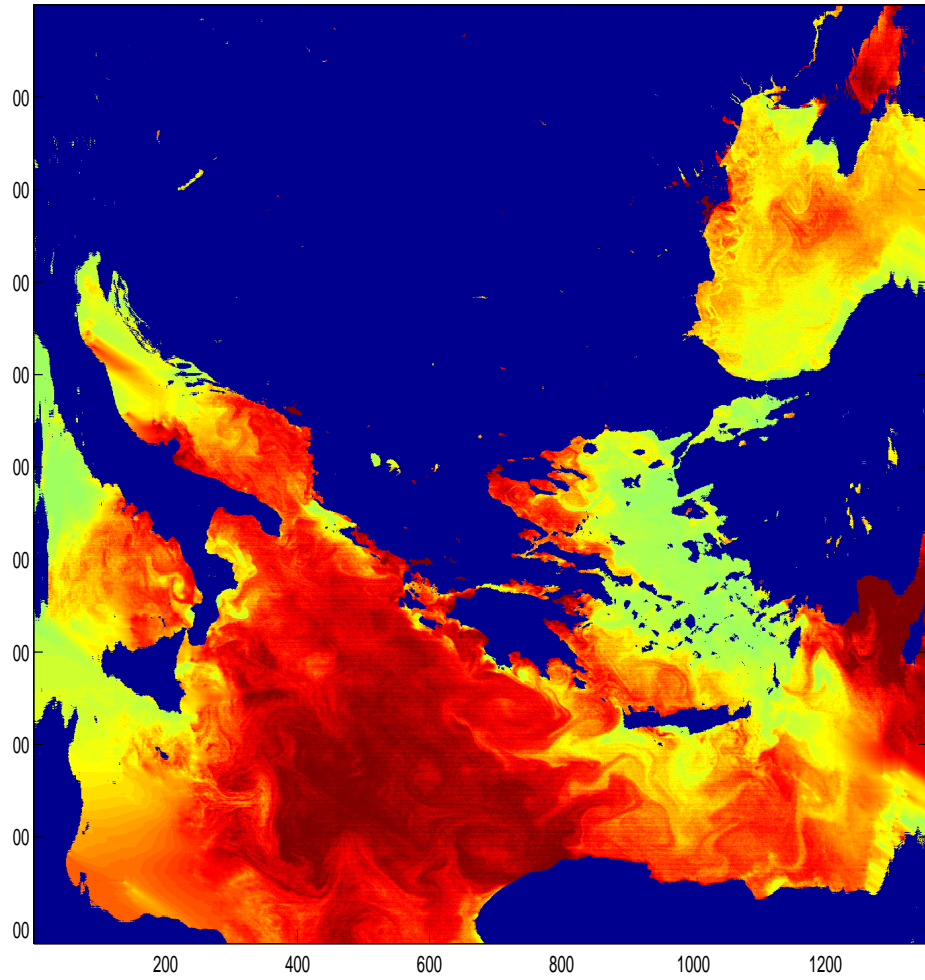
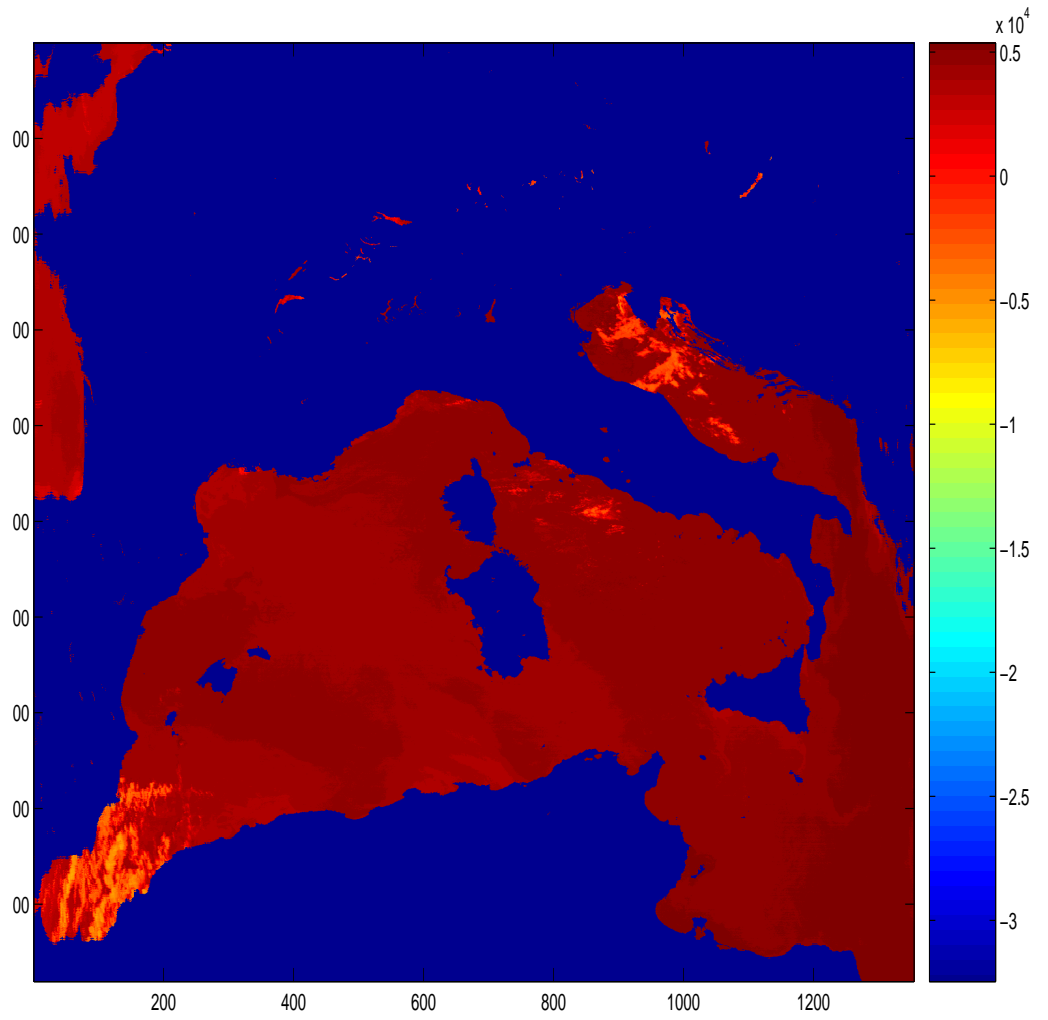Figure 6.2: After Adaptive Histogram Modification algorithm.
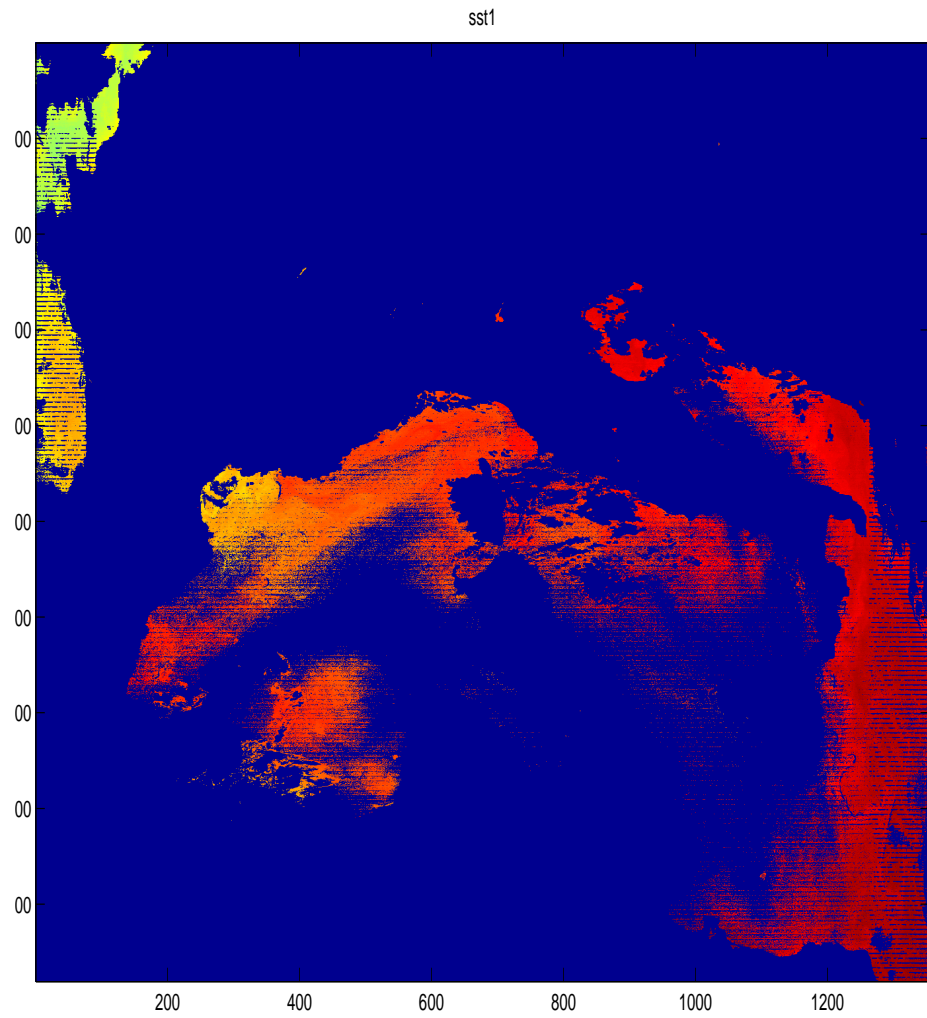
Figure 6.3: Raw SST image.
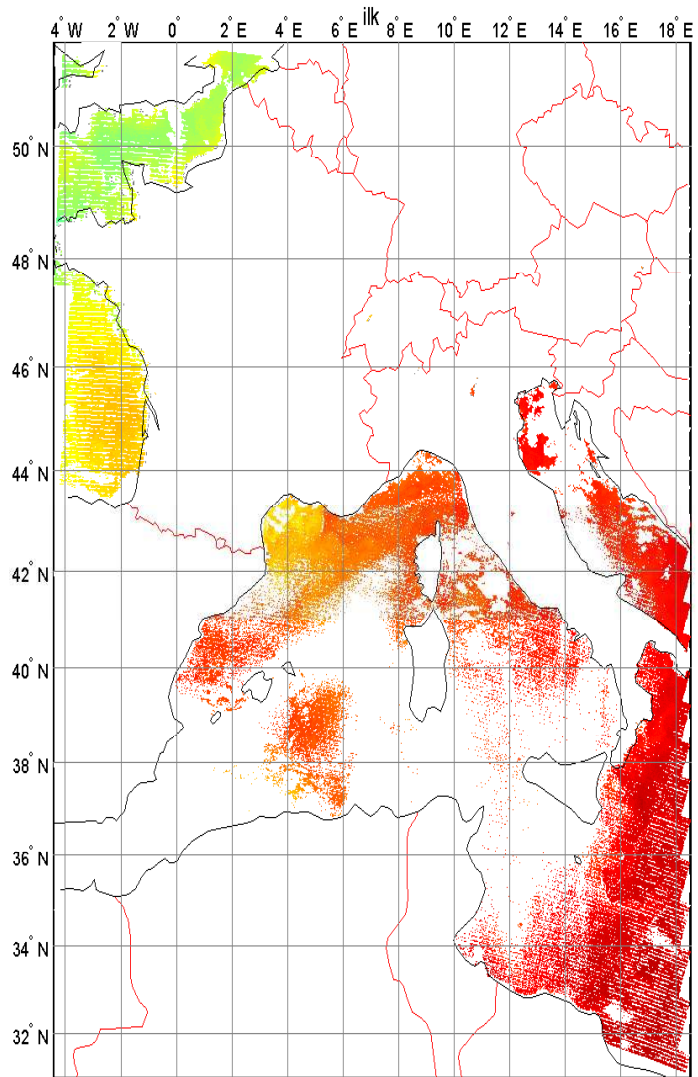
Figure 6.4: After deleting incorrect pixels.

Figure 6.5: After image to map projection our image is more understandable.

This data have about %35 inaccuracy (Figure 6.5). In Figure 6.6 below we see reconstructed image.

Since our data is now complete enough (Figure 6.6), we can try to segment in more homogenous regions.
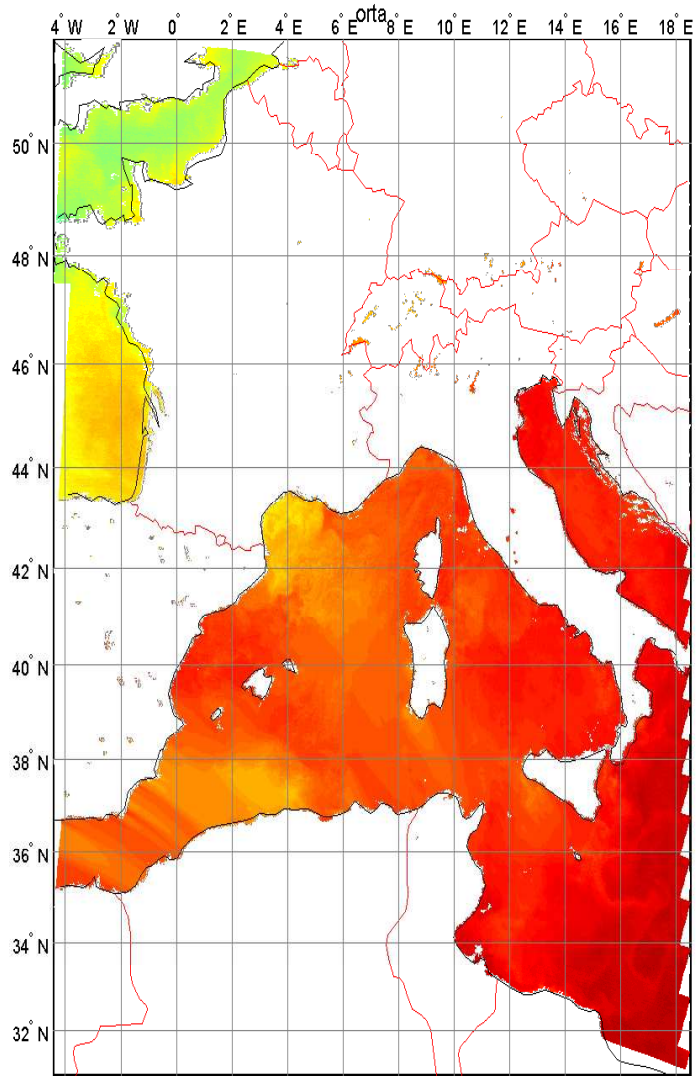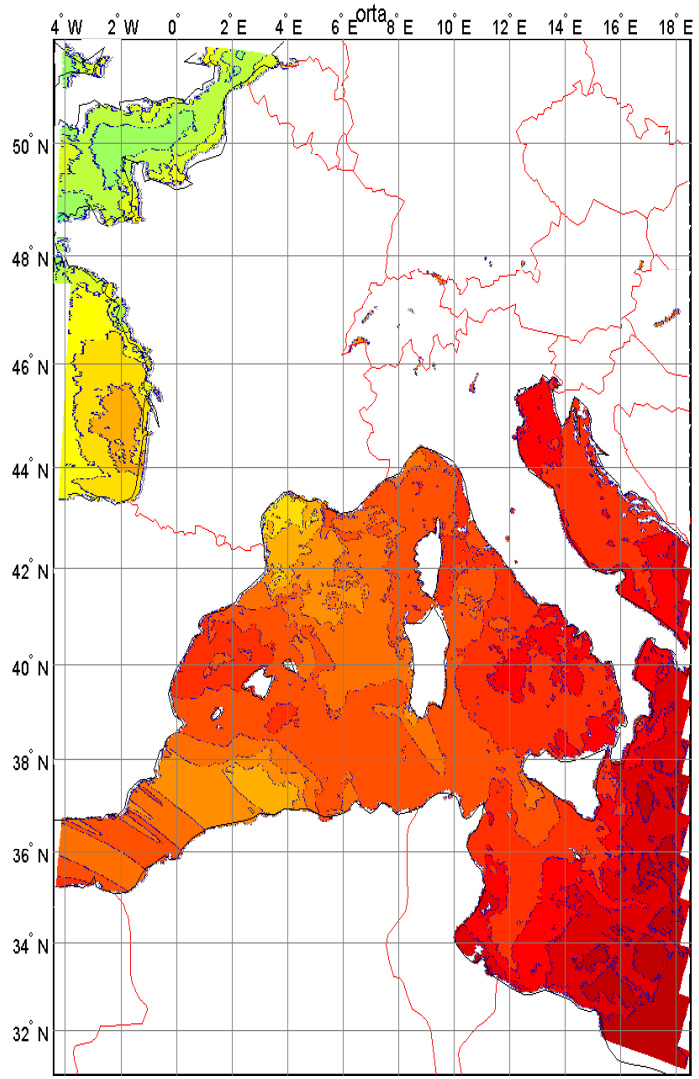
Figure 6.6: Reconstructed data.

Figure 6.7: Segmentation is done.

6.2 Future Work

Satellite sensors provide an alternative approach to measuring SST from ships, and provide the higher spatial and temporal coverage. So we generate more capable of characterizing local and seasonal SST changes, over time scales of days to years and spatial scales of a few kilometers. If used in conjunction with in situ data, i.e. from ships, moored buoys, the measurements from satellite sensors become a very powerful tool to understand many oceanographic phenomena.

Despite the undoubted applications of satellite remote sensing techniques to the study of the sea, it is true to say that for a considerable time the concept of 'oceanography from space' remained more of a promise than a reality. Sensor accuracy, cloud cover, and restricted view (little or no information on processes within the volume of the sea) are some of the reasons.

Besides it is necessary to distinguish between "bulk" and "skin" SST. Skin SST is the radiometric temperature of the sea surface, and refers to the temperature at the air-sea interface, in a thin layer of the upper microns of the ocean. Bulk SST refers to the temperature of the upper ocean mixed layer, below the oceanic skin layer. The bulk SST determined from buoy measurements is typically obtained at a depth of 1 meter.

The oceans play a key role in regulating the rate of any change in the world's climate , which has huge importance present, dedicated ocean satellites are now required.

As we mentioned before the quality of remote sensing data connected with its spatial and temporal resolutions. But in reality if a remote sensing system has high spatial resolution, its temporal resolution is low, and vice versa. So for better processing it may be useful to merge data (from separate satellites or from different bands of one sensor).

In this study we used weekly sensed SST images. Due to the fact that reconstruction algorithm of these images did not depend on time. As we reconstruct of an

incomplete image we can not get any idea about unknown pixels by using another image -from the same satellite- belongs to two weeks ago (or two weeks after). But one-day data, or fusion of data sensed same day, from different satellites, or *in situ* data may used as an approximation about missing data.

Temperature of seawater is dependent primarily upon salinity, depth, density, wind and pressure. So it is reasonable that estimating SST with the help of other data such as sea surface height (SSH), sea surface anomaly (SSA).
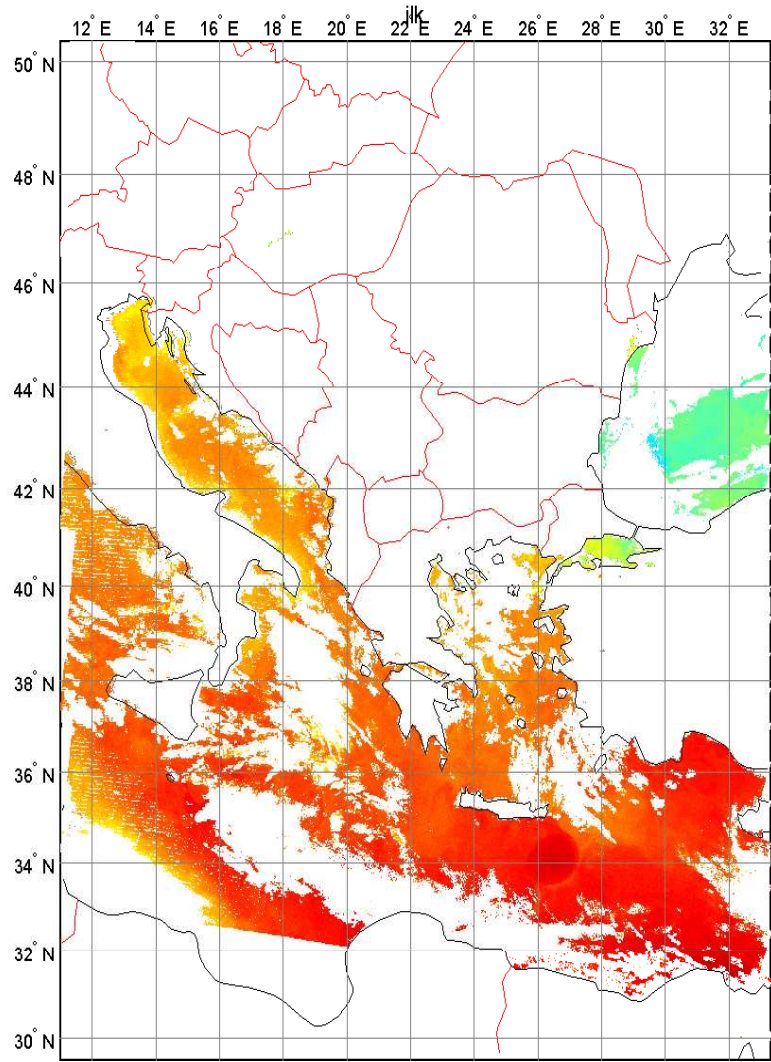
Figure 6.8: Another SST image before reconstruction end segmentation.
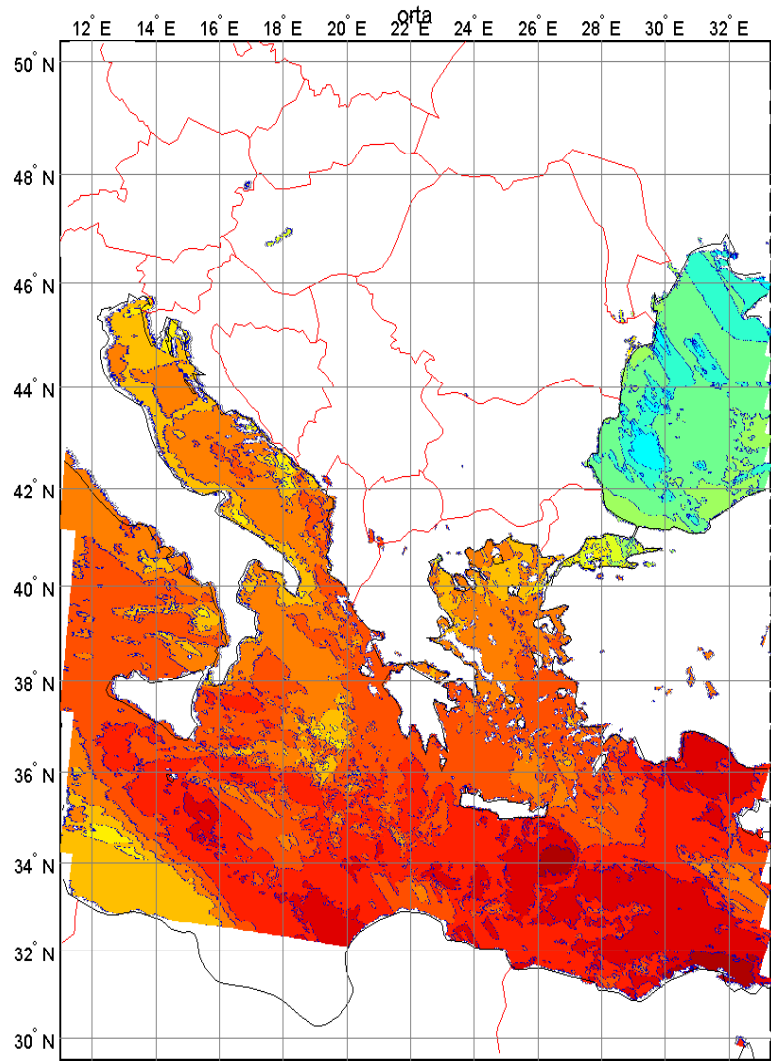
Figure 6.9: After image processing.

REFERENCES

[1] H. Öktem and Egiazarian, K., *A New Histogram Modification Method for Medical X-Ray Images*, (2002).

[2] A.K. Jain, *Fundamentals of Digital Image Processing*, Prentice Hall, 1989.

[3] A. Pekkarinen, *Image segmentation in multisource forest inventory*, Finnish Forest Research Institute, Research Papers 926, 2004.

[4] J. L. Semmlow, *Biosignal and Biomedical Image Processing MATLAB-Based Applications*, Marcel Dekker INC., New York, Basel, 2004.

[5] J. Jan, *Medical Image Processing Reconstruction and Restoration*,Taylor & Francis Group, Boca Raton London New York Singapore Concepts and Methods, 2006.

[6] K. Ray and T. Acharya, I*mage Processing Principles and Applications*, John Wiley & Sons, Inc. 2005.

[7] C. Gonzalez, E. Woods, *Digital Image Processing*, Second Edition, Prentice Hall, New Jersey, 2002.

[8] W.K. Pratt, *Digital Image Processing*, John Wiley & Sons INC., New York, 2001.

[9] J. Berne, *Practical handbook on image processing for scientific and technical applications*, 2nd ed., CRC Press, Boca Raton London New York Washington, D.C., 2004.

[10] MATLAB (R14) Help "MATLAB Function Reference".

[11] MATLAB Image Processing Toolbox.

[12] J. Serra, *Image Analysis and Mathematical Morphology*, Academic Press, New York, 1988.

[13] J. Zarowski, *An introduction to Numerical Analysis for Electrical and Computer Engineers*, John Wiley & Sons., 2004.

[14] A. Quarteroni, R. Sacco, F. Saleri, *Numerical Mathematics*, Springer, New York, 2000.

[15] S. T. Karris, *Numerical Analysis Using MATLAB and Spreadsheets*, Second Edition, Orchard publications, U.S.A. 2004.

[16] G. Deng and J. Pinoli, *Differentiation-Based Edge Detection Using the Logarithmic Image Processing Model*, Journal of Mathematical Imaging and Vision 8, 161-180 (1998).

[17] J. Starck and F. Murtagh, *Handbook of Astronomical Data Analysis*, Springer, Verlag, 2000.

[18] D. Phillips, *Image Processing in C*, R D Publications, Kansas, 2000.

[19] (eBook) - Mathematics - *Math Problems Solving With Matlab Programming.*

[20] J. L. Schafer, *Analysis Of Incomplete Multivariate Data*, CRC Press, NewYork Washington 2000.

[21] W. Collins, *Fundamental Numerical Methods and Data Analysis*, Second Edition, 2003.

[22] W. Y. Yang, Applied Numerical Methods Using Matlab., A John Wiley & Sons, 2005.

[23] G. P. Brasseur, J. J. Orlando, and G. S. Tyndall, *Atmospheric chemistry and global change*, 1. ed., Oxford University Press, New York, 1999.

[24] K. Levenberg, *A method fo the solution of certain problems in least-squares*, Quarterly Applied Math., 2, 164–168, 1944.

[25] W. G. Rees, *Physical Principles of Remote Sensing*, Second Edition, Cambridge University Press, 2001.

[26] R.M. Lewitt, *Reconstruction algorithms: Transform methods*, Proc. IEEE, vol. 71, pp. 390–408, March 1983.

[27] D. Early and D.G. Long, *Image reconstruction and enhanced resolution imaging from irregular samples*, submitted to TGARRS, 2000.

[28] S.F. Gull and G.J. Daniell, *Image reconstruction from incomplete and noisy data*, Nature, 1978.

[29] R.L. Lagendijk and J. Biemond, *Iterative Identification and Restoration of Images*, Kluver Academic Publishers, 1991.

[30] D.E. Myers , I*nterpolation and estimation with spatially located data*, Chemometrics and Intelligent Laboratory Systems, 11, 209–228, 1991.

[31] D. Anding and R. Kauth, *Estimation of sea surface temperature from space*, Remote Sens. Environ., Vol. 1, pp. 217–220, 1970.

[32] W. L. Barnes, T. Pagano, and V. V. Salomonson, *Prelaunch characteristics of the Moderate Resolution Imaging Spectroradiometer (MODIS)*, 1998.

[33] I. J. Barton, M. Zavody, D. M. OBrien, D. R. Cutten, R. W. Saunders, and D. T. Llewellyn-Jones, *Theoretical algorithms for satellite-derived sea surface temperatures*, J. Geophys. Res., vol. 94, p. 3365, 1989.

[34] H. R. Gordon, *Removal of atmospheric effects from satellite imagery of the oceans*, Appl. Opt., Vol. 17, pp. 1631–1636 ,1978.

[35] H. R. Gordon, T. Du, and T. Zhang, *Remote sensing ocean color and aerosol properties: resolving the issue of aerosol absorption*, Appl. Opt., 1997.

[36] F. Bryan and D. Thomas, *Overview of MODIS/Aqua Ocean Color Processing & Distribution*, May 2005.

[37] G. Aubert and P.Kornprobst, *Mathematical Problems in Image Processing*, Springer, New York, 2000.

[38] J. Besag, *On the statistical analysis of dirty pictures*, Journal of the Royal Statistical Society, 48(3): 259–302, 1986.

[39] F. C. Tonyand and A. V. Luminita, *Active contours without edges*, IEEE Trans. on Image Proc., 10(2): 266–277, February 2001.

[40] W. Feller, *An Introduction to Probability Theory and Its Applications*, Volume II. John Wiley & Sons, Inc., 2 edition, 1966.

[41] A. Nagy, A. Kuba, and M. Samal, *Reconstruction of factor structures using discrete tomography method*, Electronic Notes in Discrete Mathematics, 20: 519–534, 2005.

[42] Y. Rubner, C. Tomasi, and J. Guibas, *The earth movers distance as a metric for image retrieval*, International Journal of Computer Vision, 40(2) :99–121, 2000.

[43] P. Simoncelli, *Statistical models for images: Compression, restoration and synthesis*, In 31st Asilomar Conf. on Signals, Systems, and Computers, Pacific Grove, CA IEEE Sig. Proc. Soc., 1997.

[44] J. Shi and J. Malik, *Normalized cuts and image segmentation*, IEEE Trans. Patt. Anal. Mach. Intell., 22(8): 888–905, 2000.

[45] I. T. Young, J. Gerbrands, and J. van Vliet, *Fundamentals of Image Processing*, Netherlands, 1995.

[46] *Fundamentals of Remote Sensing*, Remote Sensing Tutorial, Canada Centre for Remote Sensing, Natural Resources, Canada http://www.ccrs.nrcan.gc.ca/ccrs

[47] T. M. Lillesand and R. W. Kiefer, *Remote Sensing and Image Interpretation*, University of Wisconsin, John Wiley & Sons, 2000.

[48] E. Green, P. Mumby, A. Edwards, and C. Clark, *Remote Sensing Handbook for Tropical Coastal Management*, Coastal Management Sourcebooks 3, UNESCO, Paris, 2000.

[49] F. Meyer and S. Boucher , *Morphological Segmentation". Journal of Visual Communication and Image representation*, Academic Press, 1990.

[50] J. R. Jensen, *Introductory Digital Image Processing: A Remote Sensing Perspective*, Prentice Hall, New Jersey, 1996.

[51] A. Bovik, *Handbook of Image and Video Processing*, Academic Press, New York ,Boston, 2000.

[52] A. Ardeshir Goshtasby, *2-D and 3-D Image Registration for Medical, Remote Sensing, and Industrial Applications*, John Wiley & Sons, 2005.

http://oceancolor.gsfc.nasa.gov/DOCS.

http://oceancolor.gsfc.nasa.gov/PRODUCTS/.

http://oceancolor.gsfc.nasa.gov/DOCS/MSL12/.

http://oceancolor.gsfc.nasa.gov/DOCS/MSL12/CODE/.

MODIS Algorithm Theoretical Basis Document: MOD17, MOD25, MOD28.

Appendix A

MATLAB Code for Conversion of HDF

```
% (C) Müserref TÜRKMEN

% This algorithm convert hdf file to matrix

%( size = number of scan lines * pixel per scan line)

hdfile = 'A2002203012500.L2-LAC-SST.x.hdf'

hInfo = hdfinfo(hdfile);

myfile=hInfo.Filename;

namequal-sst=hInfo.Vgroup(1,2).SDS(1,2).Name;

aqual-sst=hInfo.Vgroup(1,2).SDS(1,2).Dims(1,1).Size;

bqual-sst=hInfo.Vgroup(1,2).SDS(1,2).Dims(2,1).Size;

qual-sst = hdfread(myfile,namequal-sst,'Index', [1.0 1.0 ],[1.0 1.0 ],[aqual-sst bqual-sst ]);

namesst=hInfo.Vgroup(1,2).SDS(1,1).Name;

asst=hInfo.Vgroup(1,2).SDS(1,1).Dims(1,1).Size;

bsst=hInfo.Vgroup(1,2).SDS(1,1).Dims(2,1).Size;

sst = hdfread(myfile,namesst,'Index', [1.0 1.0 ],[1.0 1.0 ],[asst bsst ]);

namel2flags=hInfo.Vgroup(1,2).SDS(1,3).Name;

al2flag=hInfo.Vgroup(1,2).SDS(1,3).Dims(1,1).Size;

bl2flag=hInfo.Vgroup(1,2).SDS(1,3).Dims(2,1).Size;

l2-flags = hdfread(myfile,namel2flags,'Index', [1.0 1.0 ],[1.0 1.0 ],[al2flag bl2flag ]);
```

```
namelon=hInfo.Vgroup(1,3).SDS(1,1).Name;

alon=hInfo.Vgroup(1,3).SDS(1,1).Dims(1,1).Size;

blon=hInfo.Vgroup(1,3).SDS(1,1).Dims(2,1).Size;

longitude = hdfread(myfile,namelon,'Index', [1.0 1.0 ],[1.0 1.0 ],[alon blon ]);

namelat=hInfo.Vgroup(1,3).SDS(1,2).Name;

alat=hInfo.Vgroup(1,3).SDS(1,2).Dims(1,1).Size;

blat=hInfo.Vgroup(1,3).SDS(1,2).Dims(2,1).Size;

latitude = hdfread(myfile,namelat,'Index', [1.0 1.0 ],[1.0 1.0 ],[alat blat ]);

latitude=imresize(double(latitude),.1);

longitude=imresize(double(longitude),.1);

maplat2=double(hInfo.Attributes(1,28).Value);

maplat1=double(hInfo.Attributes(1,46).Value);

maplon1=double(hInfo.Attributes(1,26).Value);

maplon2=double(hInfo.Attributes(1,44).Value);

sst=double(sst);

%we eliminate unqualified pixels

sst1=sst;

qual-sst=double(qual-sst);

maxqual=max(max(qual-sst));

for  i=1:size(qual-sst,1)

for j=1:size(qual-sst,2)

if  qual-sst(i,j)==maxqual-1 — qual-sst(i,j)==maxqual
```

```
sst(i,j)=NaN;

if sst1(i,j)¡=-32760

sst(i,j)=0;

end

end

end

end

%slope = 0.0049999999f ;intercept = 0.f ;

%to convert a 16 bit [-32768 ,32767] pixel value to $^{0}C$

sst=0.005*sst;

% we calculate the percentage of incomplete data. (about % 20 is OK)

cii=0;

cnan=0;

for i=1:size(sst,1);

for j=1:size(sst,2)

if  isnan(sst(i,j))

cnan=cnan+1;

elseif sst(i,j)¿0

cii=cii+1;

end

end

end
```

accu=(100*cnan)/(i*j)

%image to map projection

mercatorm(sst,maplat2,maplat1,maplon1,maplon2,latitude,longitude);

MATLAB Code for Histogram Modification

% (C) Hakan ÖKTEM

% Adaptive Histogram Modification algorithm.

function [oupt,outt]=adtstr(img,itop,ibot,ilef,irig,sfvl,clipsize,gamm,nofbins,sensiv);

%itop,ibot,ilef,irig = offsets they are for preventing the effect of the

%sides of the image with too much noise for a 2024x2024 image taking all

%around 50 is OK

%sfvl = will be added to input data histogram. 2-3 is generally appropriate

%if there are not big gaps in the histogram it can be taken 0

%clipsize = legth of the clipping window to remove the outliers 3 is an

%appropriate choice

%gamm= constant for span adjustment. Main parameter. 0 ¡ gamm ¡ 1. I was
setting it by trial and error

%nofbins= number of the bins in the histogram generally 256 but can be

%increased if better accuracy is desired

%calculate the size of the image and selected portion

[aa,bb]=size(img);

usm=itop+1;

alm=aa-ibot;

slm=ilef+1;

sgm=bb-irig;

%normalize the image

```matlab
img=double(img);

img=img-min(min(img));

img=img/max(max(max(img)),2*eps);

%clip the data

%find min of local maxes and max of local mins

%this is necessary for eliminating the effects of extreme values

%which may occur due to the scattering of x-ray photons of limited dose

minofmax=1;

maxofmin=0;

for i=1:clipsize:aa-clipsize,

for j=1:clipsize:bb-clipsize,

minofmax=min(minofmax,max(max(img(i:i-1+clipsize,j:j-1+clipsize))));

maxofmin=max(maxofmin,min(min(img(i:i-1+clipsize,j:j-1+clipsize))));

end

end

%make clipping

img=max(img,minofmax);

img=min(img,maxofmin);

%normalize

img=img-min(min(img));

img=img/max(max(max(img)),2*eps);

%compute the input histogram
```

hgrm=himhist(img(usm:alm,slm:sgm),nofbins);

%add sfvl to conserve the real differences partially

hgrm=hgrm+sfvl;

%find the mins and maxes of the selected window

immin=min(min(min(img(usm:alm,slm:sgm))));

immax=max(max(max(img(usm:alm,slm:sgm))),2*eps);

%calculate the span for distributing the selected portion data

oupmin=gamm*immin;

oupmax=1-((1-immax)*gamm);

inrang=immax-immin;

ourang=oupmax-oupmin;

%perform the desired point transformation

totl=sum(sum(hgrm));

oupt=(oupmin/max(immin,2*eps))*min(img,immin);

for i=1:nofbins,

oupt=oupt+((ourang/max(inrang,2*eps))*(hgrm(i)/totl)*nofbins*min(img-(((i-1)*inrang)/no
immin,(inrang/nofbins)).*(img¿(((((i-1)*inrang)/nofbins)+immin)));

end

oupt=oupt+((1-oupmax)/max(1-immax,2*eps))*(img-immax).*(img¿immax);

%normalize

oupt=oupt-min(min(oupt));

oupt=oupt/max(max(max(oupt)),2*eps);

% the selected area based histogram flattening is completed up to here % after here "% %" is the comment line and % is for the code lines using unavailable data

% % histogram mapping stage

% load trgt;

hgrm=hgrm-sfvl;

totl=sum(sum(hgrm));

avrg=totl/nofbins;

trggt=hgrm.*(hgrm¿(avrg*sensiv));

nwsiz=sum(hgrm¿(avrg*sensiv));

trgt=zeros([nwsiz,1]);

inds=1;

% % read the target histogram to the array "trgt". "trgt.mat" is assumed to have the desired histogram which is not available yet

for i=1:nofbins,

if trggt(i)¿0.5,

trgt(inds)=trggt(i);

inds=inds+1;

end

end

trgtot=sum(trgt);

outt=min(oupt,oupmin);

lvv=oupmin;

```
for i=1:nwsiz,

outt=outt+(trgtot/(trgt(i)*nwsiz))*min(oupt-lvv,trgt(i)*ourang/trgtot).*(oupt¿lvv);

lvv=lvv+trgt(i)*ourang/trgtot;

end

outt=outt+(oupt-oupmax).*(oupt¿oupmax);

outt=outt-min(min(outt));

outt=outt/max(max(max(outt)),2*eps);
```

MATLAB Code for Reconstruction

% this algorithm finds unknown pixels of incomplete SST image

% This algorithm is called in converthdf.m so we do not write parameters again.

for i=2:size(sst,1)

for j=2:size(sst,2)

if isnan(sst(i,j))

count=0;

count1=0;

count2=0;

count3=0;

count4=0;

value=0;

iminusa1=0;

iplusa2=0;

jminusb1=0;

jplusb2=0;

%we try to figure out known pixels at the same row or column with missing pixel

for a=i-1:-1:1

% in this stage we eliminate pixels wrt distance between missing pixel

%we start from the most northest, westest, eastest and southest pixels

%our aim is to find nearest pixel in the direction.

% we research for all 4 direction if ĩsnan(sst(i-a,j)) & sst(i-a,j)¿0

```
count=1;

count1=1;

iminusa1=sst(i-a,j);

x1=a;

end

end

for b=j-1:-1:1

if ĩsnan(sst(i,j-b)) & sst(i,j-b)¿0

count2=1;

if count1==0

count=1;

else

count=2;

end

jminusb1=sst(i,j-b);

y1=b;

end

end

for a=size(sst,1)-i:-1:1

if ĩsnan(sst(i+a,j)) & sst(i+a,j)¿0

count3=1;

if count1+count2==2
```

```
count=3;

elseif count1+count2==1

count=2;

else

count=1;

end

iplusa2=sst(i+a,j);

x2=a;

end

end

for b=size(sst,2)-j:-1:1

if ĩsnan(sst(i,j+b)) & sst(i,j+b)¿0

count4=1;

if count1+count2+count3==3

count=4;

elseif count1+count2+count3==2

count=3;

elseif count1+count2+count3==1

count=2;

else

count=1;

end
```

jplusb2=sst(i,j+b);

y2=b; end

end

% we approximate the missing pixel using known pixels...

% count is the number of known pixel.

% we search only 4 direction, $(count_max = 4)$

if count==4

alpha=1+x1/x2+x1/y1+x1/y2;

sst(i,j)=(x1/alpha)*(iminusa1*1/x1+iplusa2*1/x2+jminusb1*1/y1+jplusb2*1/y2);

elseif count==3 & jminusb1==0

alpha=1+x1/x2+x1/y2;

sst(i,j)=(x1/alpha)*(iminusa1*1/x1+iplusa2*1/x2+jplusb2*1/y2);

elseif count==3 & iplusa2==0

alpha=1+x1/y1+x1/y2;

sst(i,j)=(x1/alpha)*(iminusa1*1/x1+jminusb1*1/y1+jplusb2*1/y2);

elseif count==3 & jplusb2==0

alpha=1+x1/x2+x1/y1;

sst(i,j)=(x1/alpha)*(iminusa1*1/x1+iplusa2*1/x2+jminusb1*1/y1);

elseif count==3 & iminusa1==0

alpha=1+x2/y1+x2/y2;

sst(i,j)=(x2/alpha)*(iplusa2*1/x2+jminusb1*1/y1+jplusb2*1/y2);

elseif count==2 & iminusa1==0

```
if iplusa2==0

alpha=1+y1/y2;

sst(i,j)=(y1/alpha)*(jminusb1*1/y1+jplusb2*1/y2);

elseif jminusb1==0

alpha=1+x2/y2;

sst(i,j)=(x2/alpha)*(iplusa2*1/x2+jplusb2*1/y2);

elseif jplusb2==0

alpha=1+x2/y1;

sst(i,j)=(x2/alpha)*(iplusa2*1/x2+jminusb1*1/y1);

end

elseif count==2 & iplusa2==0

if jminusb1==0

alpha=1+x1/y2;

sst(i,j)=(x1/alpha)*(iminusa1*1/x1+jplusb2*1/y2);

elseif jplusb2==0

alpha=1+x1/y1;

sst(i,j)=(x1/alpha)*(iminusa1*1/x1+jminusb1*1/y1);

end

elseif count==2 & jminusb1==0

if jplusb2==0

alpha=1+x1/x2;

sst(i,j)=(x1/alpha)*(iminusa1*1/x1+iplusa2*1/x2);
```

end

end

end

end

end

Appendix B

Properties of data:

Name: A2007099002500.L2-LAC-SST.x.hdf

Title: MODISA Level-2 Data

Sensor Name: MODISA

Product Name: A2007099002500.L2-LAC-SST

Software Name: MSl12 (name of the software used to create this product.)

Software Version: 5.6.5 (version of the software used to create this product.)

Replacement Flag: ORIGINAL

Orbit Node Longitude: 0 (longitude at equatorial crossing of day-side node).

Orbit Number: 0 (orbit number of the scene.)

Node Crossing Time:

Processing Time: 2007107052624000 local time of generation of this product; concatenated digits for year, day-of-year, hours, minutes, seconds, and fraction of seconds in the format of YYYYDDDHHMMSSFFF.

Creation Time: 2007117210812000

Processing Control: MSl12 (path and name of the file containing the control parameters. This information is stored in the product as part of its processing history.)

par=/data1/vdc/sdpsoper/vpu0/workbuf/A2007099002500.L1B-LAC.param

metafile=A2007099002500.L2-LAC.meta

Input Parameters:

IFILE1 = /data1/vdc/sdpsoper/vpu0/workbuf/A2007099002500.L1B-LAC

OFILE1 = A2007099002500.L2-LAC-SST

L2PROD1 = sst, qual-sst, l2-flags

CALFILE = CLDFILE = GEOFILE =/data1/vdc/sdpsoper/vpu0/workbuf/A2007099002500.

GEO RFLAG = ORIGINAL

EVAL = 0

MODE = 0

SPIXL = 1

EPIXL = -1

DPIXL = 1

SLINE = 1

ELINE = -1

DLINE = 1

CTL-PT-INCR = 8

PROC-OCEAN = 1

PROC-LAND = 0

ATMOCOR = 1

AER-OPT = -3

AER-WAVE-SHORT = 748

AER-WAVE-LONG = 869

AER-SWIR-SHORT = -1

AER-SWIR-LONG = -1

AER-ITER-MAX = 10

BRDF-OPT = 7

GAS-OPT = 1

IOP-OPT = 0

GSM01-OPT = 0

GSM01-FIT = 0

QAA-OPT = 0

QAA-S = 0.01500

POL-OPT = 3

ABSAER-OPT = 0

SL-PIXL = -1

SL-FRAC = 0.2500

GLINT-OPT = 1

RESOLUTION = -1

OUTBAND-OPT = 2

OXABAND-OPT = 0

FILTER-OPT = 1

FILTER-FILE = /sdps/sdpsoper/data/OCDATA/data/modisa/msl12-filter.dat

FILTER-1 = 7 x 5 (1) straylight filter on flag 5

FILTER-2 = 7 x 5 (1) straylight filter on flag 10

MET1 = /data1/vdc/sdpsoper/vpu0/workbuf/S200709900-NCEP.MET

MET2 = /data1/vdc/sdpsoper/vpu0/workbuf/S200709906-NCEP.MET

MET3 = /data1/vdc/sdpsoper/vpu0/workbuf/S200709906-NCEP.MET

OZONE1 = /data1/vdc/sdpsoper/vpu0/workbuf/S20070980009823-TOAST.OZONE

OZONE2 = /data1/vdc/sdpsoper/vpu0/workbuf/S20070990009923-TOAST.OZONE

OZONE3 = /data1/vdc/sdpsoper/vpu0/workbuf/S20070990009923-TOAST.OZONE

LAND = /sdps/sdpsoper/data/OCDATA/data/common/landmask.dat

WATER = /sdps/sdpsoper/data/OCDATA/data/common/watermask.dat

DEMFILE = /sdps/sdpsoper/data/OCDATA/data/common/digital-elevation-map.hdf

ICEFILE = /sdps/sdpsoper/data/OCDATA/data/common/ice-mask.hdf

SSTFILE = /data1/vdc/sdpsoper/vpu0/workbuf/oisst.20070411

NO2FILE = /sdps/sdpsoper/data/OCDATA/data/common/no2-climatology.hdf

ALPHAFILE = /sdps/sdpsoper/data/OCDATA/data/common/alpha510-climatology.hdf

TAUAFILE = /sdps/sdpsoper/data/OCDATA/data/common/taua865-climatology.hdf

GAIN = 0.9710, 0.9848, 0.9795, 0.9870, 0.9850, 0.9797, 0.9776, 0.9855, 1.0000

OFFSET = 0.00000, 0.00000, 0.00000, 0.00000, 0.00000, 0.00000, 0.00000, 0.00000, 0.00000

AERMODELS = o99, m50, m70, m90, m99, c50, c70, c90, c99, t50, t90, t99

TAUA = 0.0000, 0.0000, 0.0000, 0.0000, 0.0000, 0.0000, 0.0000, 0.0000, 0.0000

AERMODRAT = 0.00000

AERMODMIN = -1f

AERMODMAX = -1f

ALBEDO = 0.027

ABSAER = 0.000

RHOAMIN = 0.00010

NLWMIN = 0.150

HIPOL = 0.500

WSMAX = 8.000

TAUAMAX = 0.300

EPSMIN = 0.850

EPSMAX = 1.350

GLINT-THRESH = 0.005

WINDSPEED = -1000.000

WINDANGLE = -1000.000

PRESSURE = -1000.000

OZONE = -1000.000

WATERVAPOR = -1000.000

RELHUMID = -1000.000

SUNZEN = 90.000

SATZEN = 60.000

MASKLAND = 1

MASKBATH = 0

MASKCLOUD = 1

MASKGLINT = 0

MASKSUNZEN = 0

MASKSATZEN = 0

MASKHILT = 1

MASKSTLIGHT = 0

MUMM-ALPHA = 1.945

MUMM-GAMMA = 1.000

MUMM-EPSILON = 1.000

CHLOC2-WAVE = -1, -1

CHLOC2-COEF = 0.00000, 0.00000, 0.00000, 0.00000, 0.00000

CHLOC3-WAVE = 443, 489, 550

CHLOC3-COEF = 0.28300, -2.75300, 1.45700, 0.65900, -1.40300

CHLOC4-WAVE = -1, -1, -1, -1

CHLOC4-COEF = 0.00000, 0.00000, 0.00000, 0.00000, 0.00000

CHLCLARK-WAVE = 443, 488, 551

CHLCLARK-COEF = 0.78927, -3.92552, 11.63776, -27.15800, 27.93696, -10.39859

VCAL-OPT = -1

VCAL-NLW = 0.0000, 0.0000, 0.0000, 0.0000, 0.0000, 0.0000, 0.0000, 0.0000, 0.0000

VCAL-LW = 0.0000, 0.0000, 0.0000, 0.0000, 0.0000, 0.0000, 0.0000, 0.0000, 0.0000

VCAL-CHL = -1.0000

VCAL-SOLZ = -1.0000

Input Files: (the names of the Level-1A or Level-1B file from which the current product was created and of the ancillary (environmental) data files used in the processing. This information is stored in the product as part of its processing history.)

A2007099002500.L1B-LAC,S200709900-NCEP.MET,

S200709906-NCEP.MET,S200709906-NCEP.MET,

S20070980009823-TOAST.OZONE,

S20070990009923-TOAST.OZONE,

S20070990009923-TOAST.OZONE,,,

landmask.dat,

watermask.dat,

digital-elevation-map.hdf,

ice-mask.hdf,

oisst.20070411,

no2-climatology.hdf,

alpha510-climatology.hdf,

taua865-climatology.hdf,

A2007099002500.GEO,

Mask Names: ATMFAIL, LAND, CLDICE, HILT

Number of Bands: 9

Number of Scan Lines: 1972

Pixels per Scan Line: 1354

Scene Center Scan Line: 987

Number of Scan Control Points: 1972

Number of Pixel Control Points: 1354

Start Time: 2007099002515394

Start Year: 2007

Start Day: 99

Start Millisec: 1515395

Upper Left Longitude: 10.9751

Upper Right Longitude: 41.9633

Upper Left Latitude: 50.3737

Upper Right Latitude: 45.8908

Start Center Longitude: 27.2085

Start Center Latitude: 49.2052

Latitude Units: degrees North

Longitude Units: degrees East

Scene Center Time: 2007099002741628

Scene Center Longitude: 24.0747

Scene Center Latitude: 40.5351

Scene Center Solar Zenith: 124.47

Earth-Sun Distance Correction: 0.99722

End Time: 2007099003006385

End Year: 2007

End Day: 99

End Milisec: 1806386

Lower Left Longitude: 9.1959

Lower Right Longitude: 33.3502

Lower Left Latitude: 32.9611

Lower Right Latitude: 29.4583

End Center Longitude: 21.5289

End Center Latitude: 31.816

Northernmost Latitude: 50.4293

Southernmost Latitude: 29.4583

Easternmost Longitude: 41.9929

Westernmost Longitude: 9.1959

Start Node: Descending

End Node: Descending

Day or Night: Night

Flag Percentages: 0 54.56827 0 0 0 6.868538 3.064269 0 0 0 0 0 100 0 0 0 0 0 0 0 0.4720943 0 0 0 0 0 0 32.4769 54.56827 0 0 45.43173